Supporting Information

Mechanochemical One-Pot Synthesis and Solid-State Transformation of Cobalt(II) Schiff Base Complexes: A Green Route to Tailored Coordination Architectures

Hongguang Chen, Zhenwei Guo, Daming Feng*, Xudong Jin*, Fang Guo *

College of Chemistry, Liaoning University, Shenyang 110036, China.

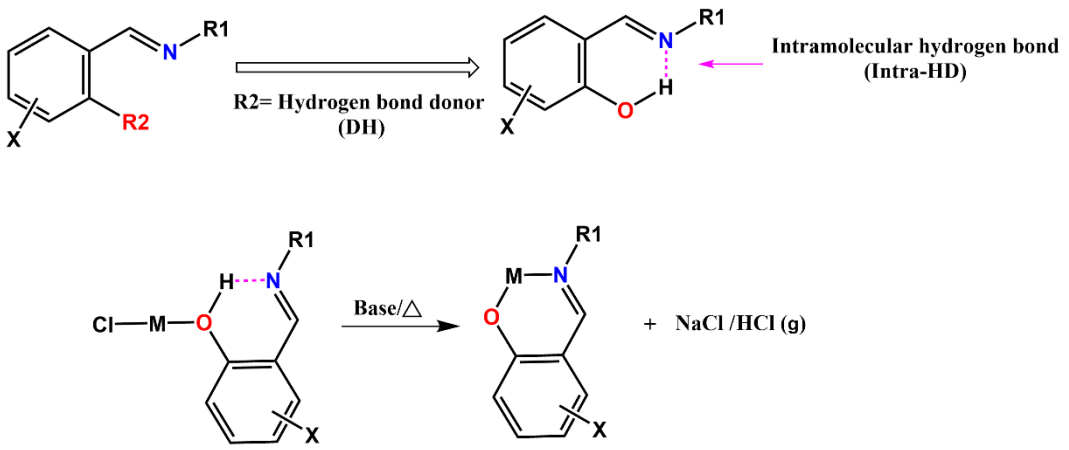

Figure S1. Schematic representation of the dehydrohalogenation of intramolecular hydrogen bonds in Schiff bases and their metal complexes

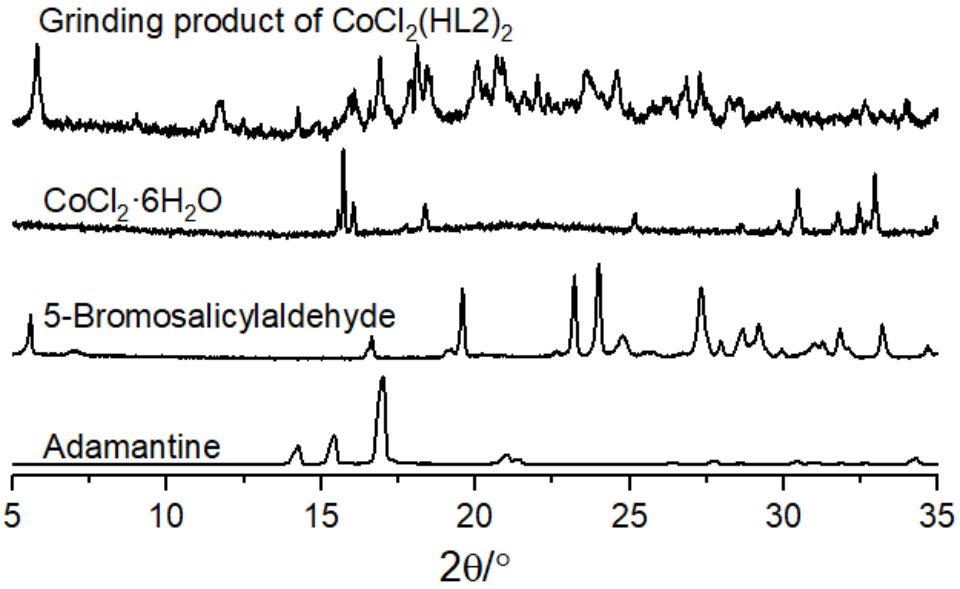

Figure S2. One-pot mechanochemical synthesis of **$CoCl_2(HL2)_2$** by neat grinding of amantadine and 5-bromosalicylaldehyde and $CoCl_2·6H_2O$ in 2:2:1 molar ratio.

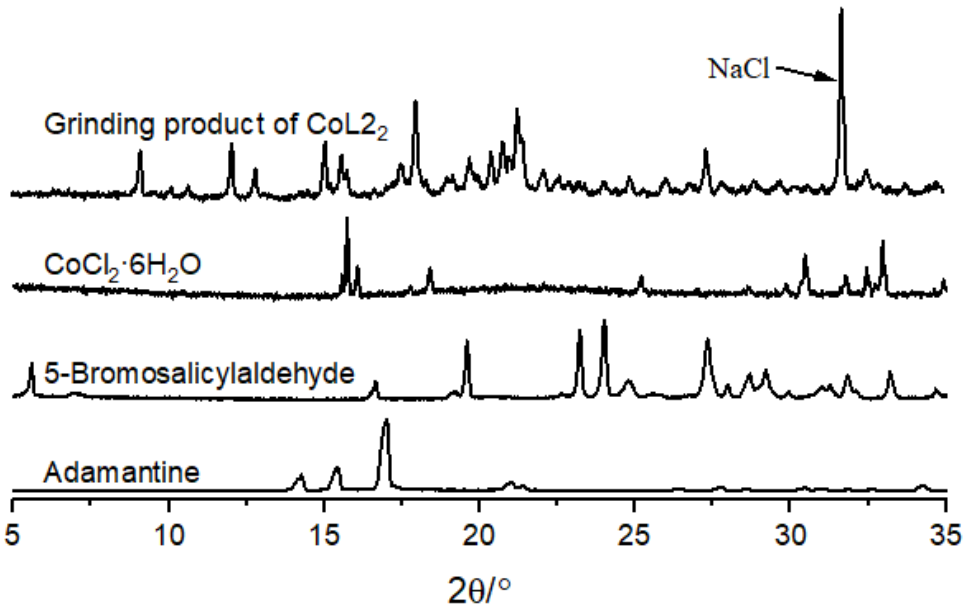

Figure S3. One-pot mechanochemical synthesis of **CoL2$_2$** by grinding of amantadine and 5-bromosalicylaldehyde, $CoCl_2 \cdot 6H_2O$ and NaOH in 2:2:2:1 molar ratio with the aid of methanol (60 uL).

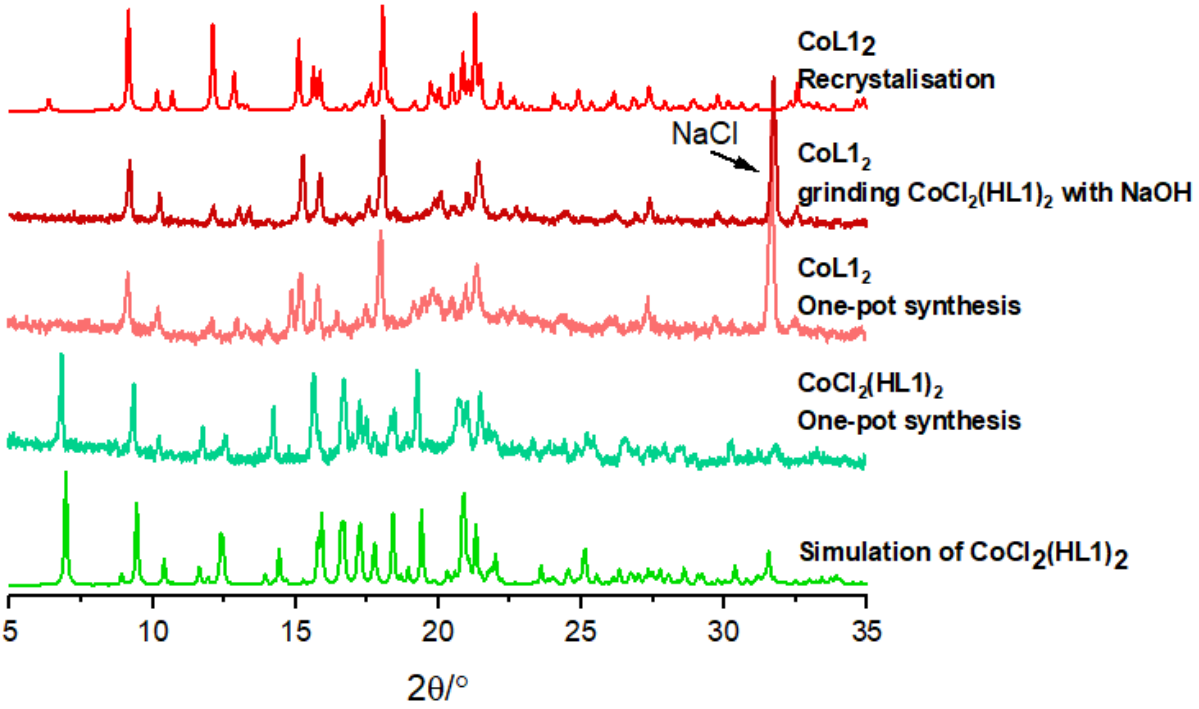

Figure S4. PXRD patterns of monodentate **CoCl$_2$(HL1)$_2$** complexes and bidentate complexes **CoL1$_2$** synthesised by mechanochemical one-pot process and dehalogenation of hydrogen.

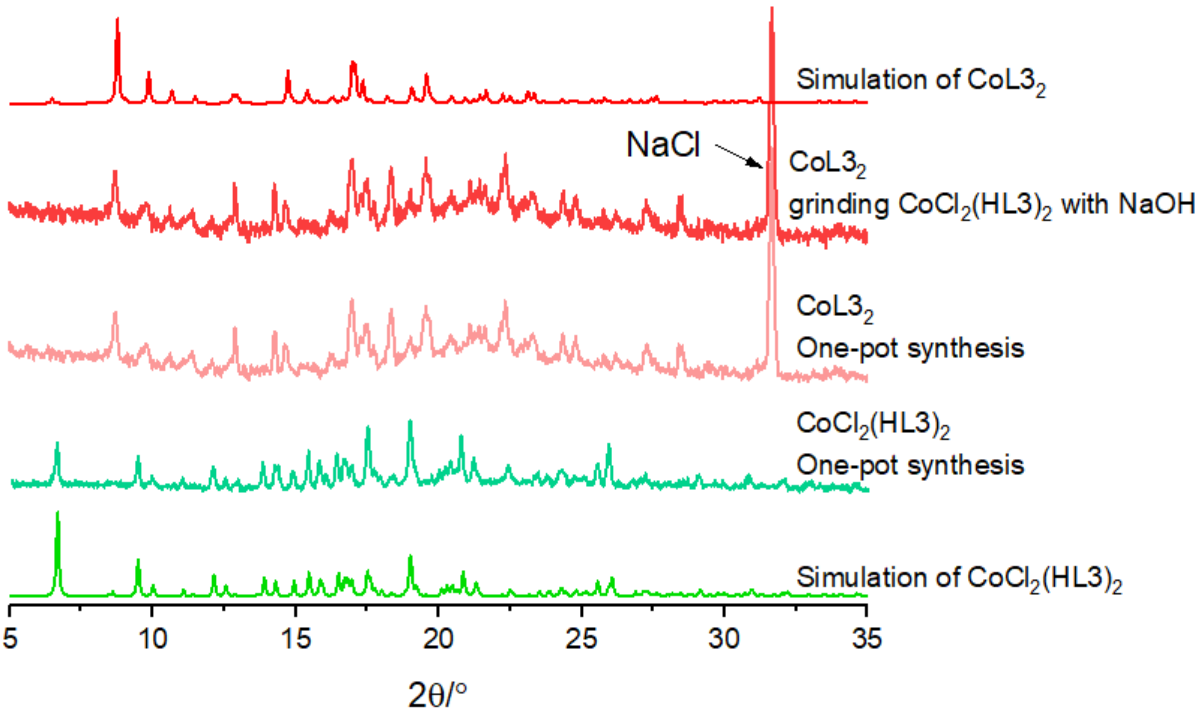

Figure S5. PXRD patterns of monodentate **$CoCl_2(HL3)_2$** complexes and bidentate complexes **$CoL3_2$** synthesised by mechanochemical one-pot process and dehalogenation of hydrogen.

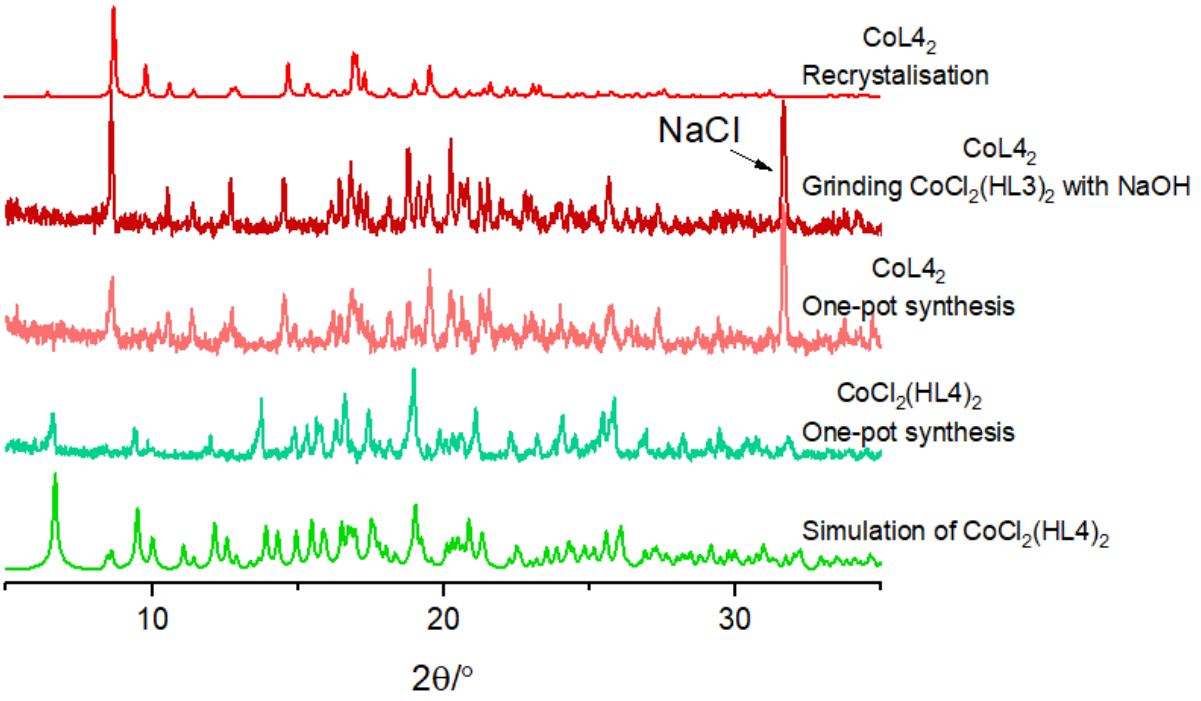

Figure S6. PXRD patterns of monodentate **$CoCl_2(HL4)_2$** complexes and bidentate complexes **$CoL4_2$** synthesised by mechanochemical one-pot process and dehalogenation of hydrogen.

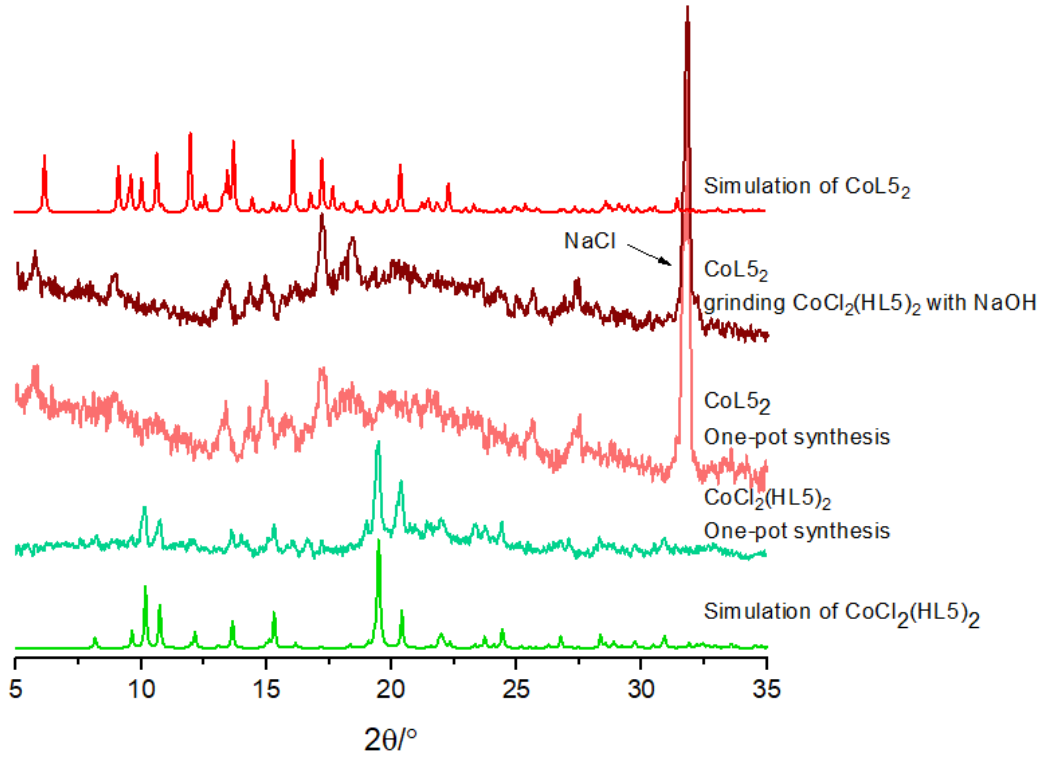

Figure S7. PXRD patterns of monodentate **$CoCl_2(HL5)_2$** complexes and bidentate complexes **$CoL5_2$** synthesised by mechanochemical one-pot process and dehalogenation of hydrogen.

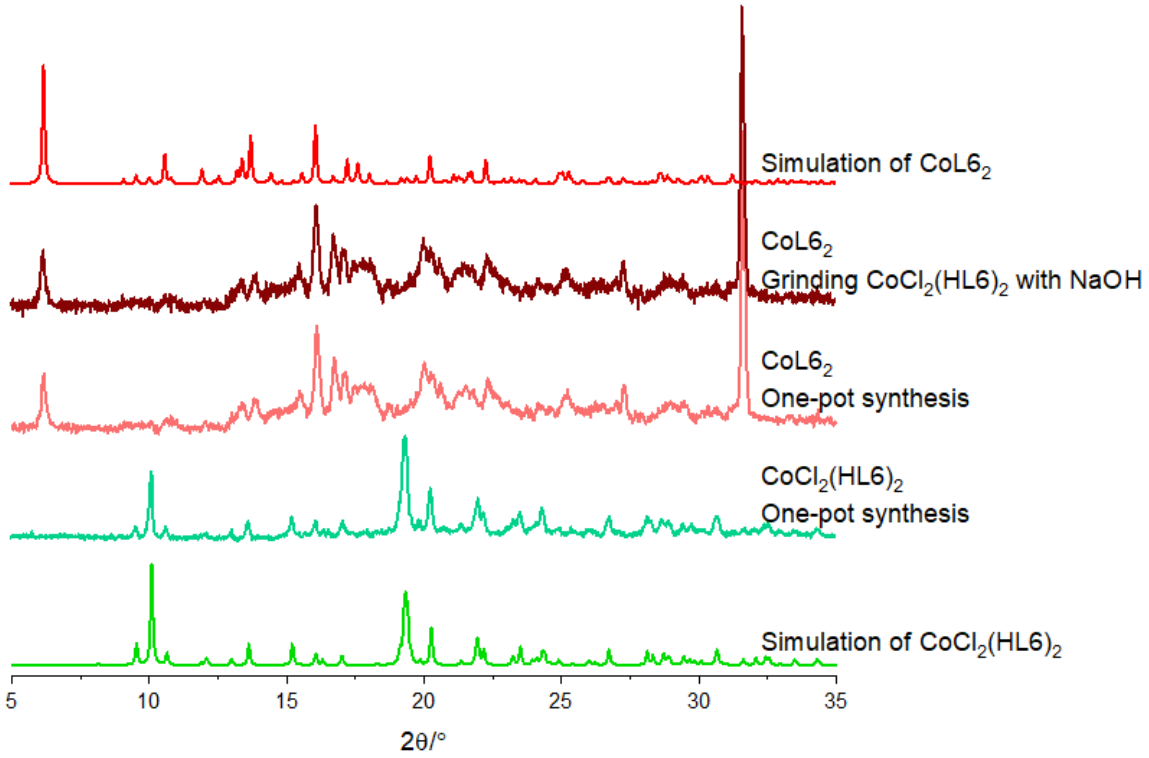

Figure S8. PXRD patterns of monodentate **$CoCl_2(HL6)_2$** complexes and bidentate complexes **$CoL6_2$** synthesised by mechanochemical one-pot process and dehalogenation of hydrogen.

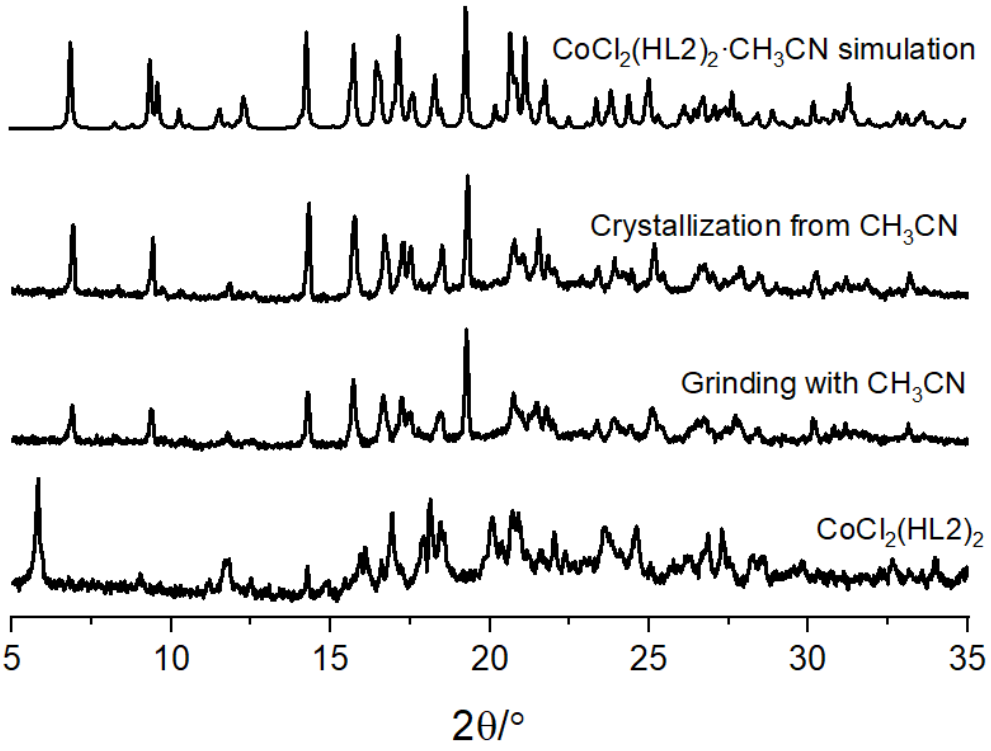

Figure S9. PXRD patterns showing the structural rearrangement of **$CoCl_2(HL2)_2$** with the involvement of acetonitrile (CH_3CN).

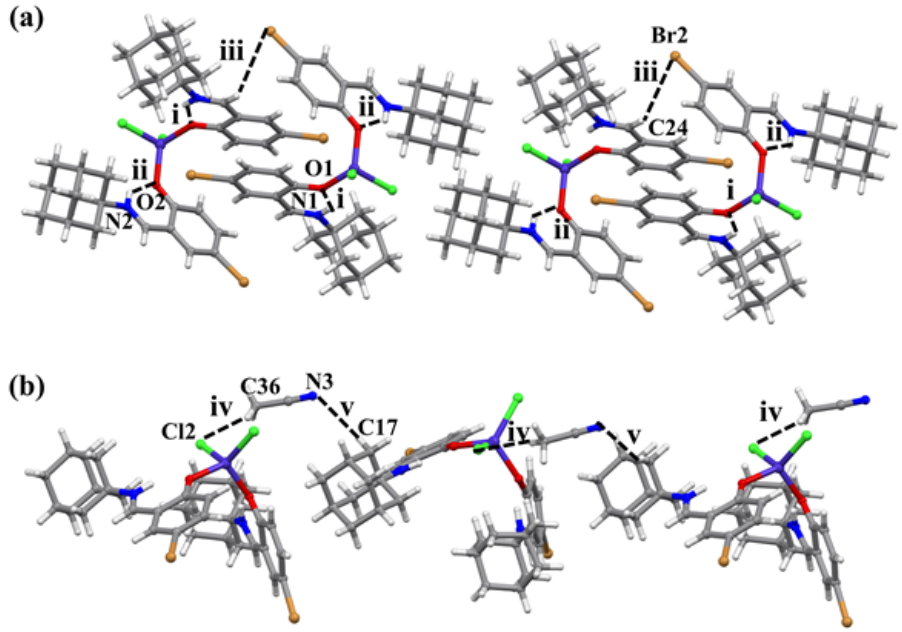

Figure S10. Crystal structures showing the charge assisted hydrogen bonding interactions in **$CoCl_2(HL2)_2 \cdot CH_3CN$**. (N1–H1···O1(i), 2.600 Å, 137.08°; N2–H2···O2(ii), 2.614 Å, 135.09°; C24–H24···Br2(iii), 3.630 Å, 154.14°; C36–H36···Cl2 (iv), 3.696 Å, 154.94°; C17–H17···N3(v), 3.573 Å, 143.77°)

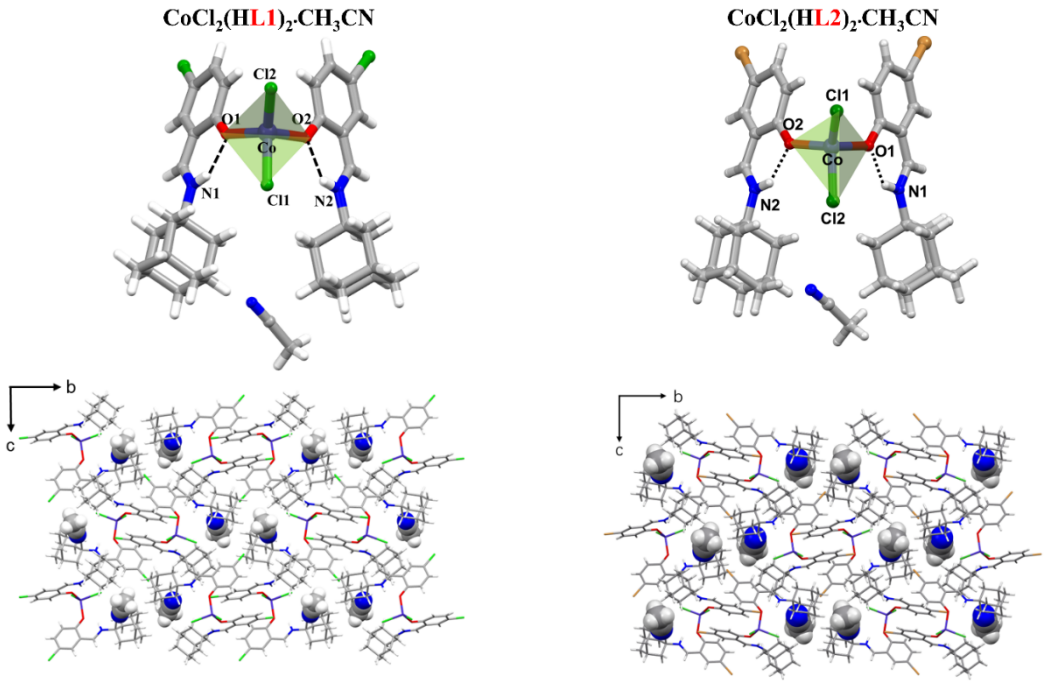

Figure S11. The crystal structures of **$CoCl_2(HL1)_2$** (left) and **$CoCl_2(HL2)_2$** (right) are depicted, along with their respective stacking modes. (blue indicates nitrogen, red indicates oxygen, grey indicates carbon, green indicates chlorine, white indicates hydrogen, violet indicates cobalt, and the green shapes represent the polyhedral tetrahedral coordination formed by cobalt.)

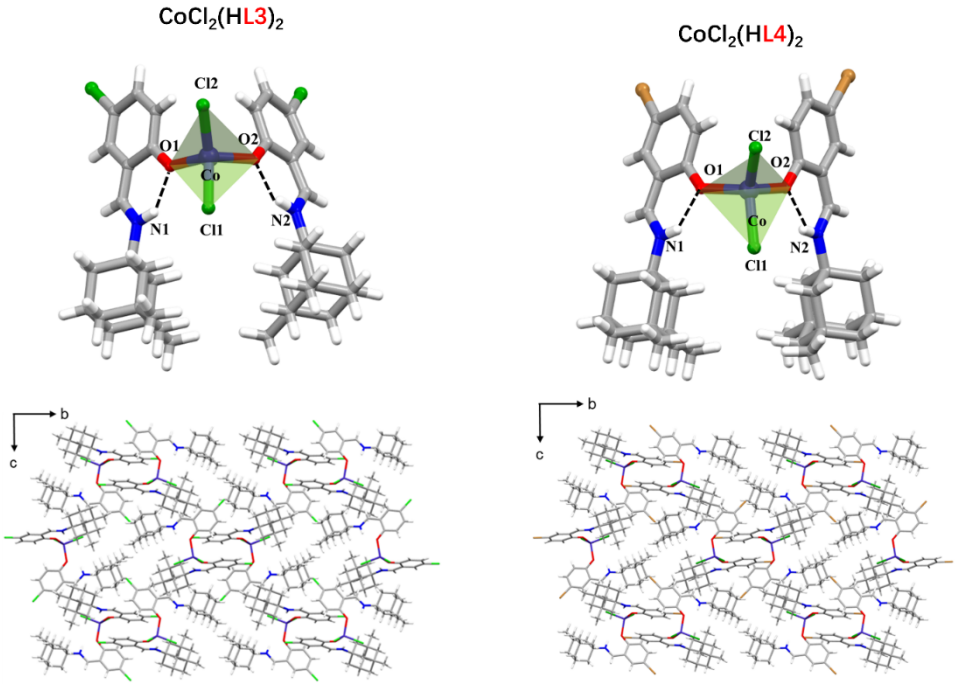

Figure S12. The crystal structures of **$CoCl_2(HL3)_2$** (left) and **$CoCl_2(HL4)_2$** (right) are depicted, along with their respective stacking modes. (blue indicates nitrogen, red indicates oxygen, grey indicates carbon, green indicates chlorine, orange indicates bromine, white indicates hydrogen, violet indicates cobalt, and the green shapes represent the polyhedral tetrahedral coordination formed by cobalt.)

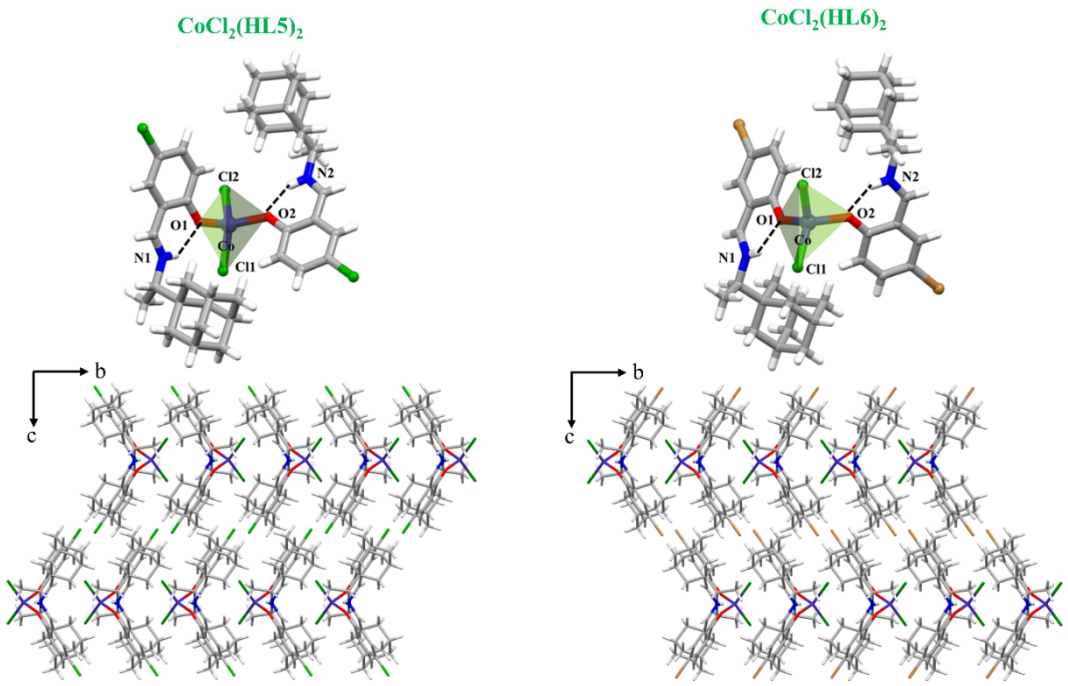

Figure S13. The crystal structures of **$CoCl_2(HL5)_2$** (left) and **$CoCl_2(HL6)_2$** (right) are depicted, along with their respective stacking modes. (blue indicates nitrogen, red indicates oxygen, grey indicates carbon, green indicates chlorine, orange indicates bromine, white indicates hydrogen, violet indicates cobalt, and the green shapes represent the polyhedral tetrahedral coordination formed by cobalt.)

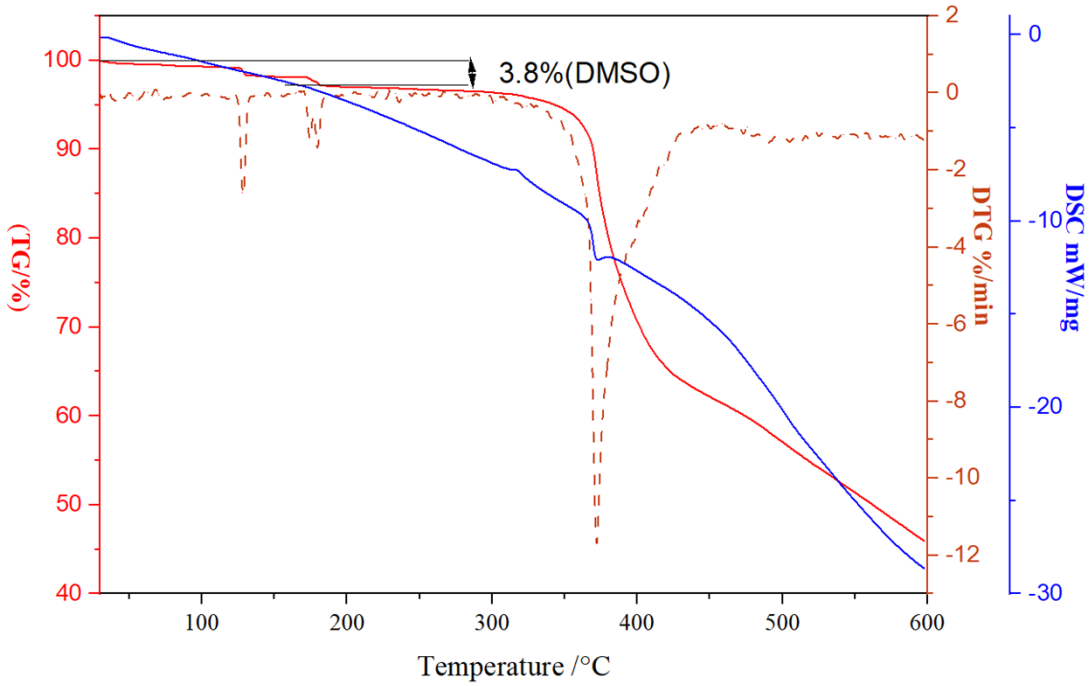

Figure. S14. TG-DSC of **$CoL2_2$**.DMSO Crystals.

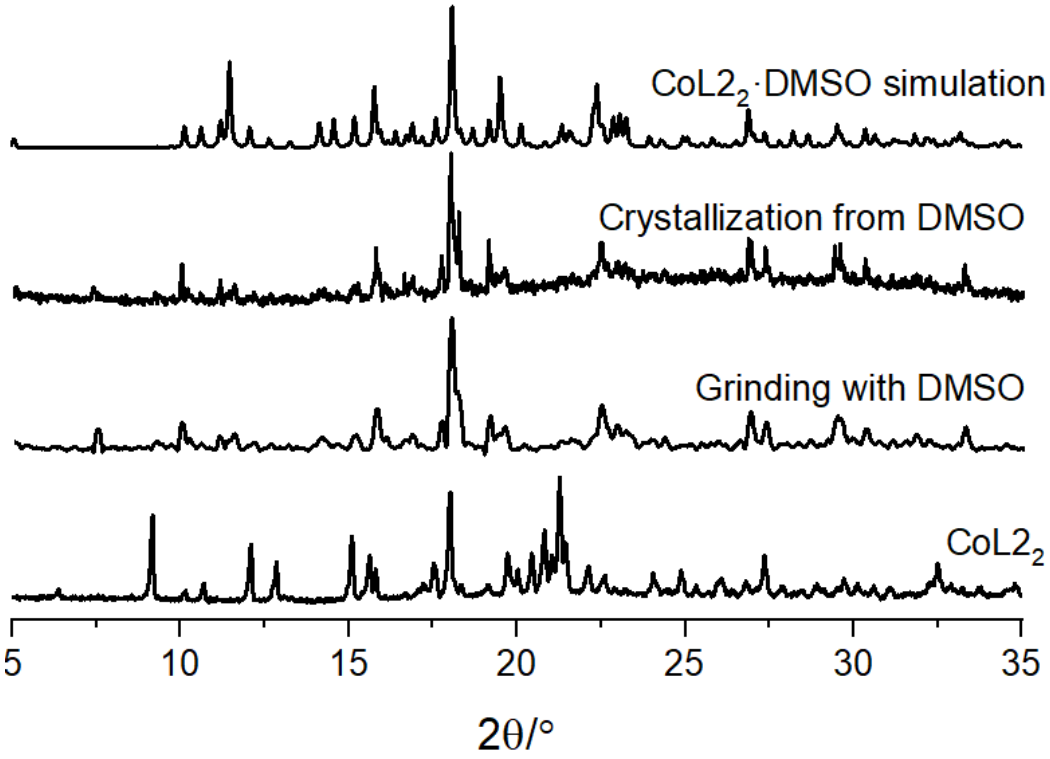

Figure S15. PXRD patterns showing the structural rearrangement of **CoL2$_2$** with the involvement of dimethyl sulfoxide (DMSO).

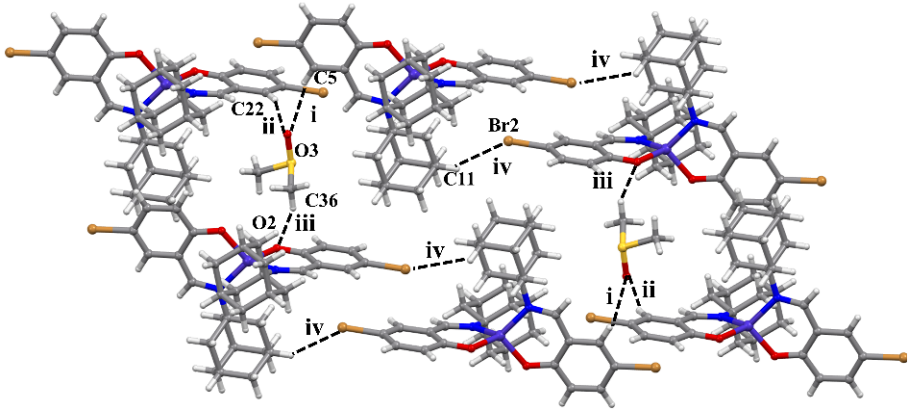

Figure S16. Crystal structures showing the charge assisted hydrogen bonding interactions in **CoL2$_2$·DMSO**. (C5–H5···O3(i), 3.481 Å, 161.05°; C22–H22···O3 (ii), 3.331Å, 158.52°; C36-H36···O2(iii), 3.553 Å, 149.72°; C36–H36···Br2(iv), 3.711 Å, 128.72°)

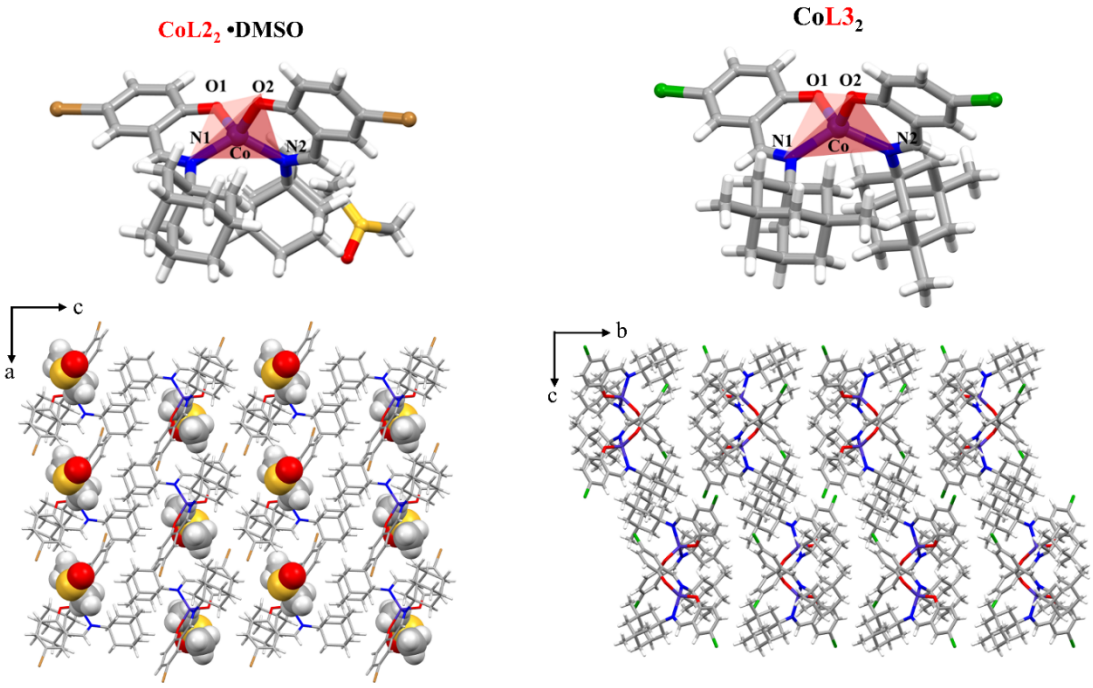

Figure S17. The crystal structures of **CoL2** (left) and **CoL3** (right) are depicted, along with their respective stacking modes. (blue indicates nitrogen, red indicates oxygen, grey indicates carbon, green indicates chlorine, orange indicates bromine, white indicates hydrogen, violet indicates cobalt, and the green shapes represent the polyhedral tetrahedral coordination formed by cobalt.)

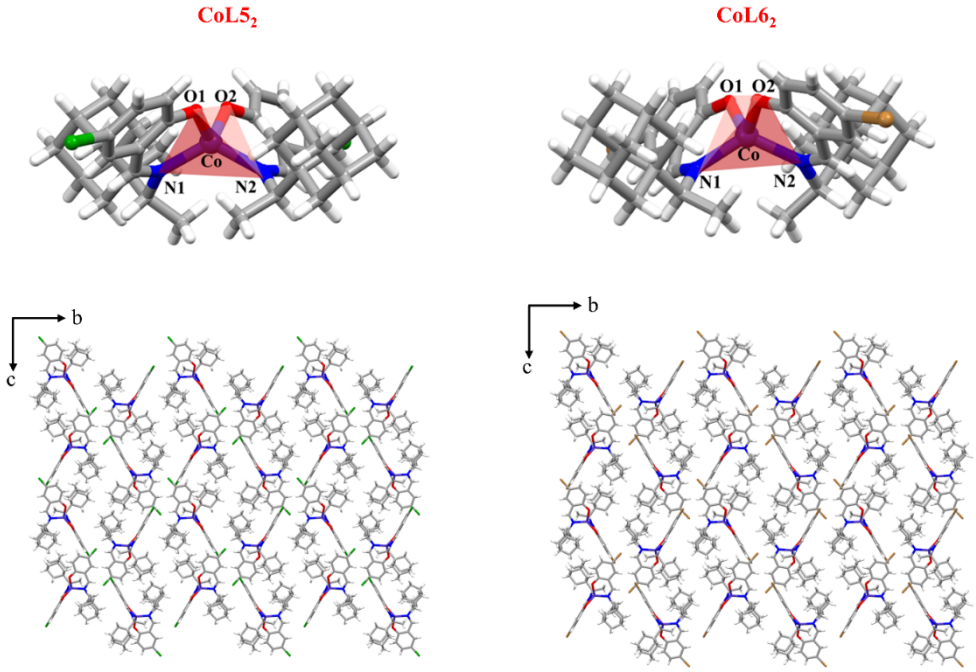

Figure S18. The crystal structures of **CoL5** (left) and **CoL6** (right) are depicted, along with their respective stacking modes. (blue indicates nitrogen, red indicates oxygen, grey indicates carbon, green indicates chlorine, orange indicates bromine, white indicates hydrogen, violet indicates cobalt, and the green shapes represent the polyhedral tetrahedral coordination formed by cobalt.).

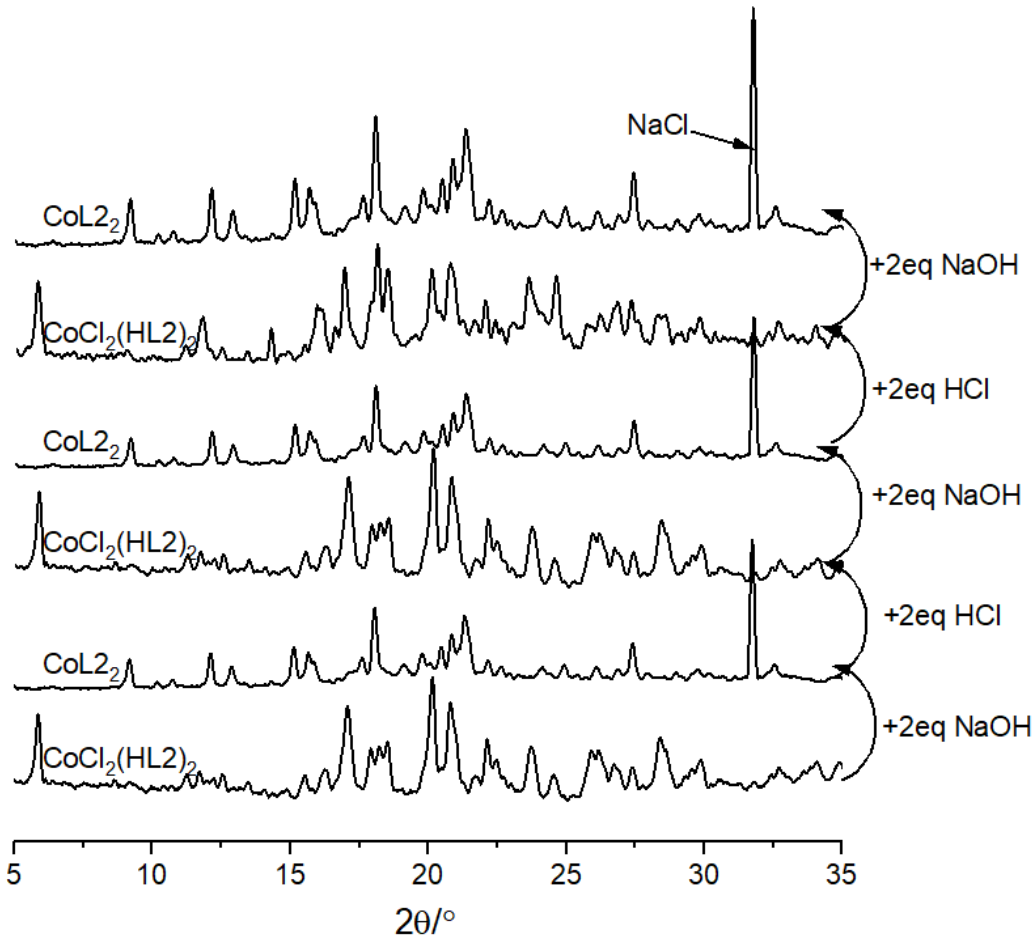

Figure S19. The PXRD patterns showing reversible solid-state transformation between **$CoCl_2(HL2)_2$** and **$CoL2_2$**.

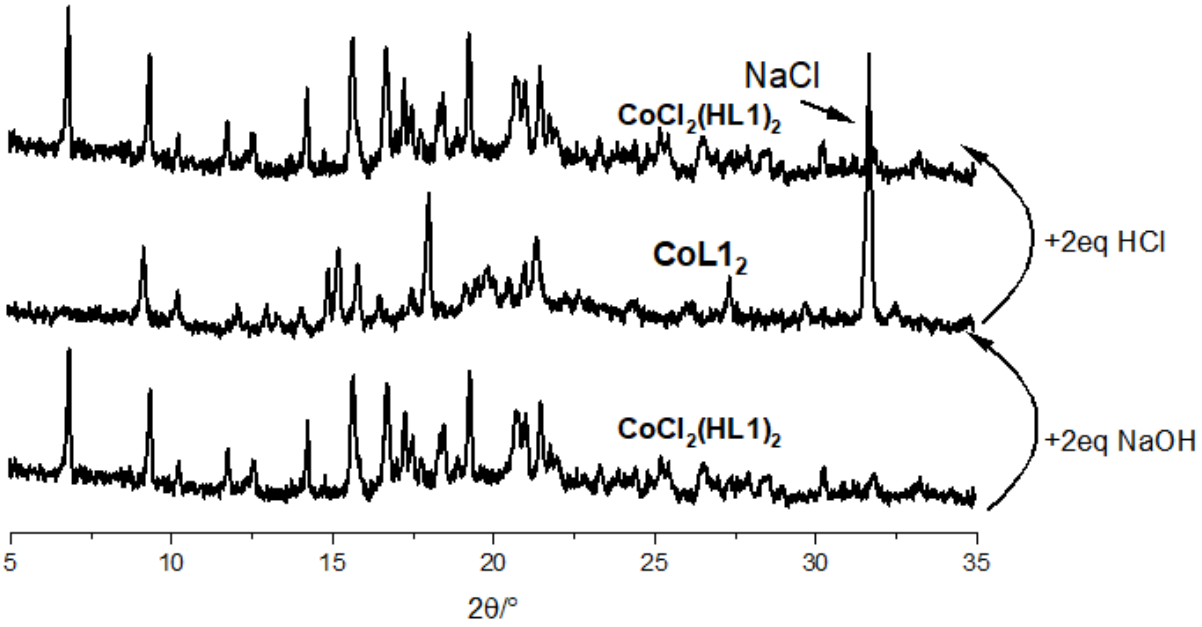

Figure S20. The PXRD patterns showing reversible solid-state transformation between **$CoCl_2(HL1)_2$** and **$CoL1_2$**.

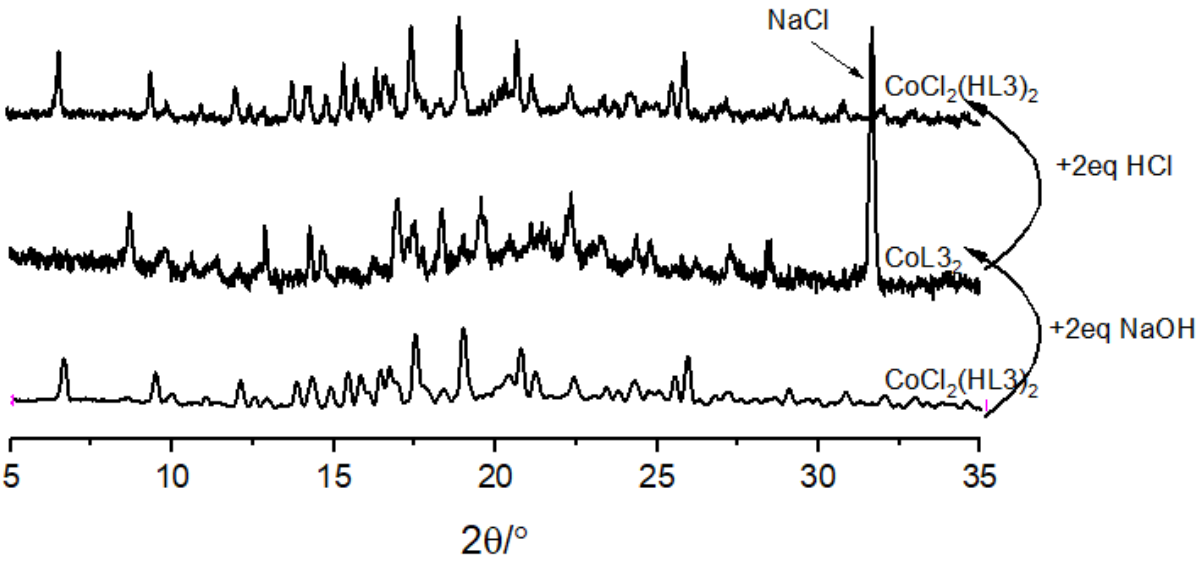

Figure S21. The PXRD patterns showing reversible solid-state transformation between **$CoCl_2(HL3)_2$** and **$CoL3_2$**.

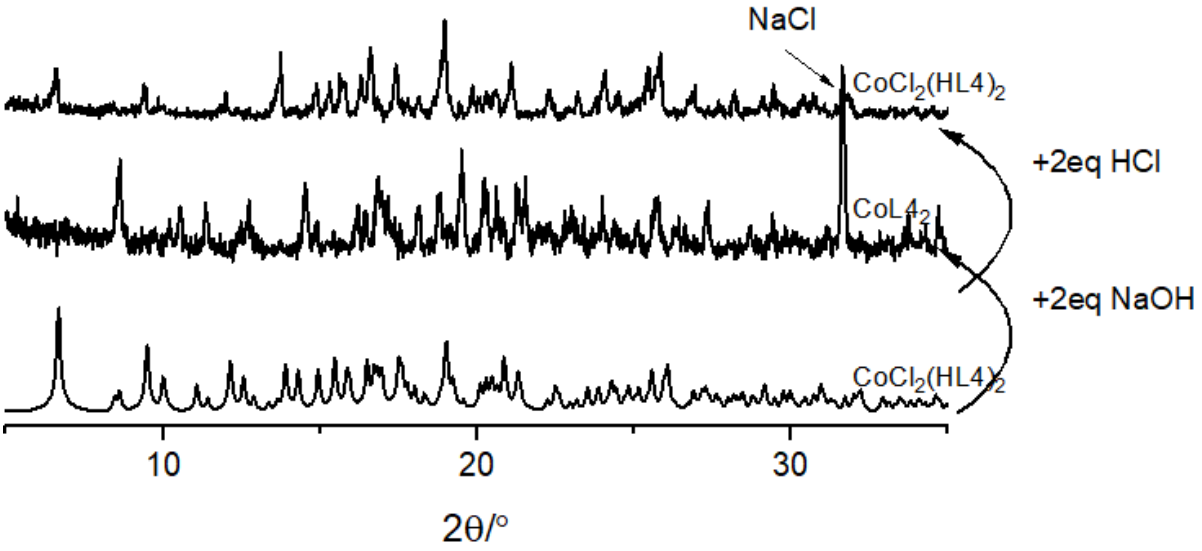

Figure S22. The PXRD patterns showing reversible solid-state transformation between **$CoCl_2(HL4)_2$** and **$CoL4_2$**.

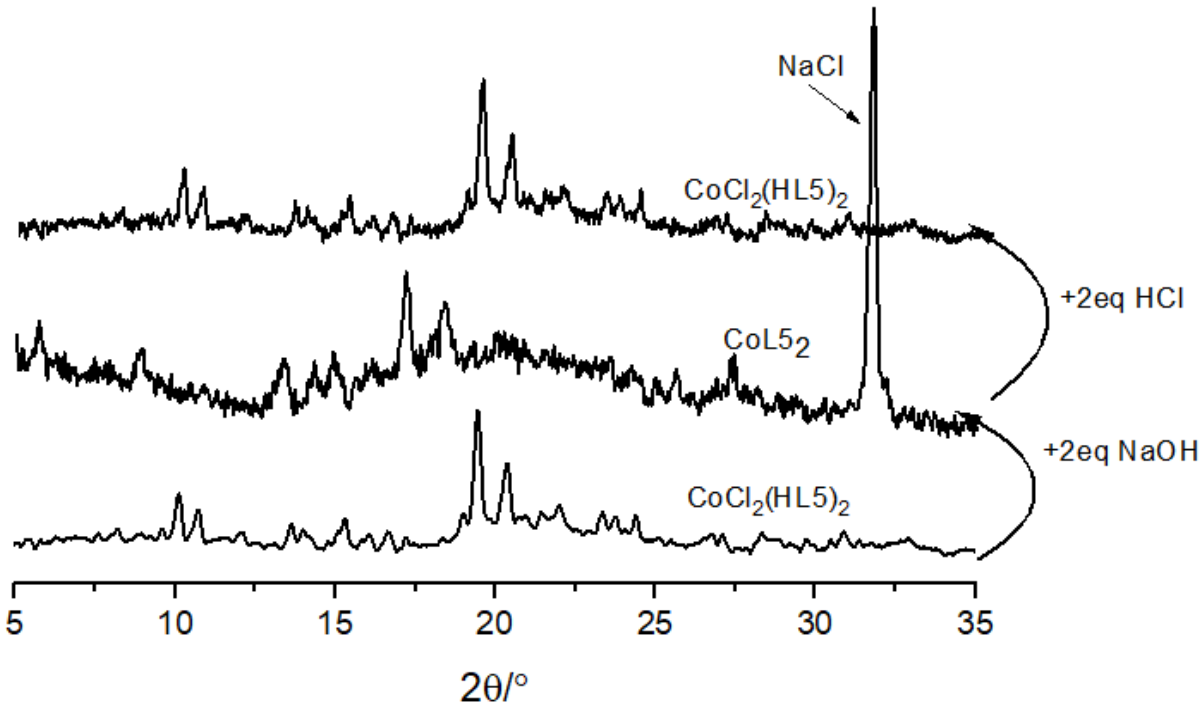

Figure S23. The PXRD patterns showing reversible solid-state transformation between **$CoCl_2(HL5)_2$** and **$CoL5_2$**.

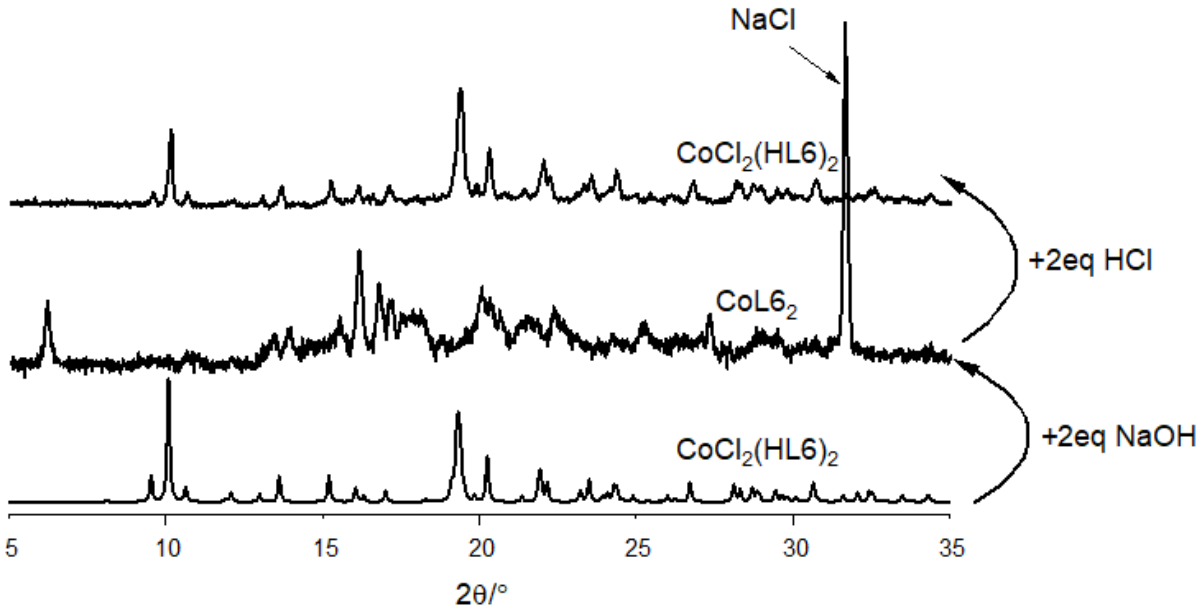

Figure S24. The PXRD patterns showing reversible solid-state transformation between **$CoCl_2(HL6)_2$** and **$CoL6_2$**

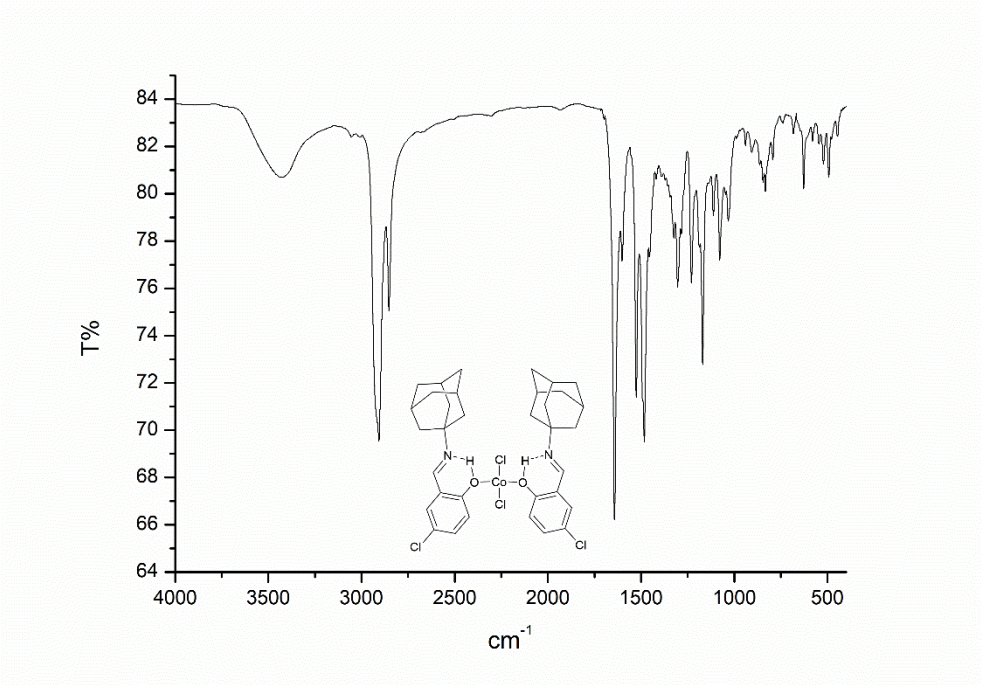

Figure S25. IR of $CoCl_2(HL1)_2$.

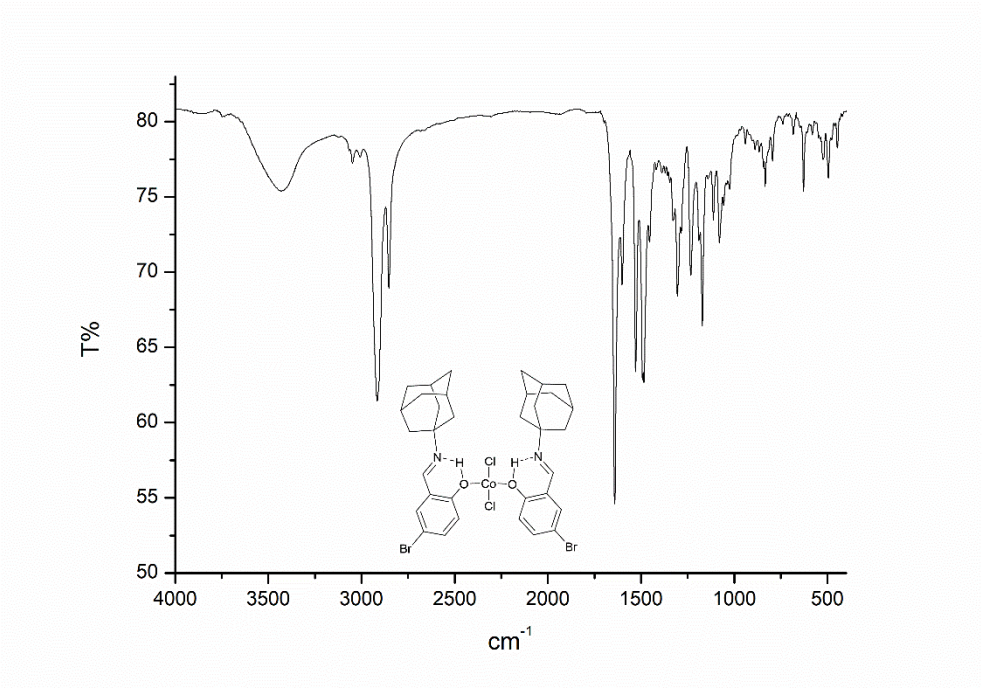

Figure S26. IR of $CoCl_2(HL2)_2$.

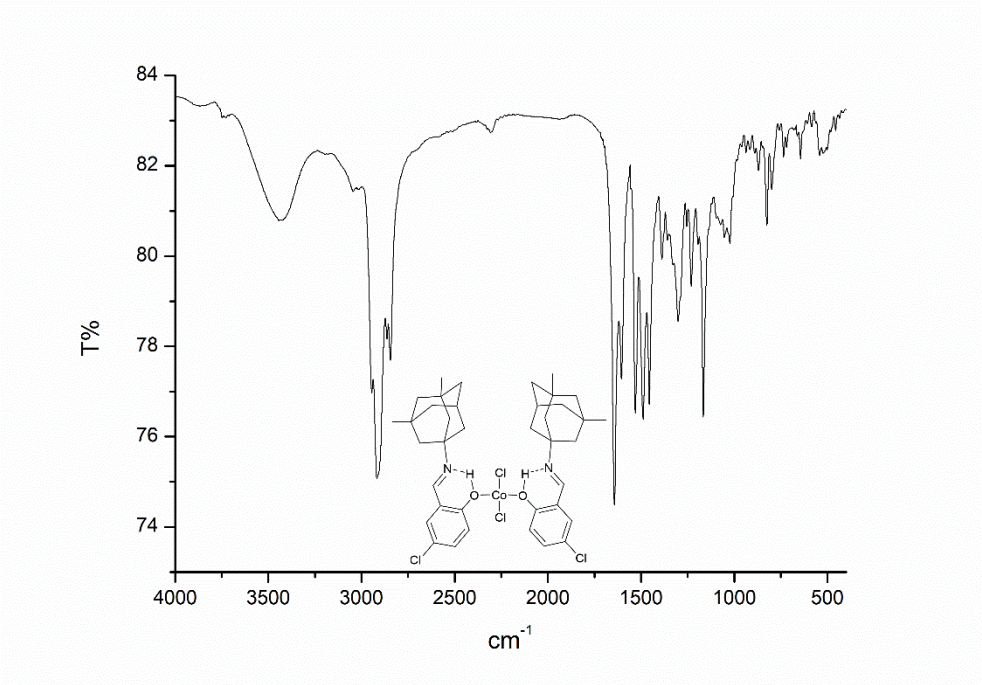

Figure S27. IR of $CoCl_2(HL3)_2$.

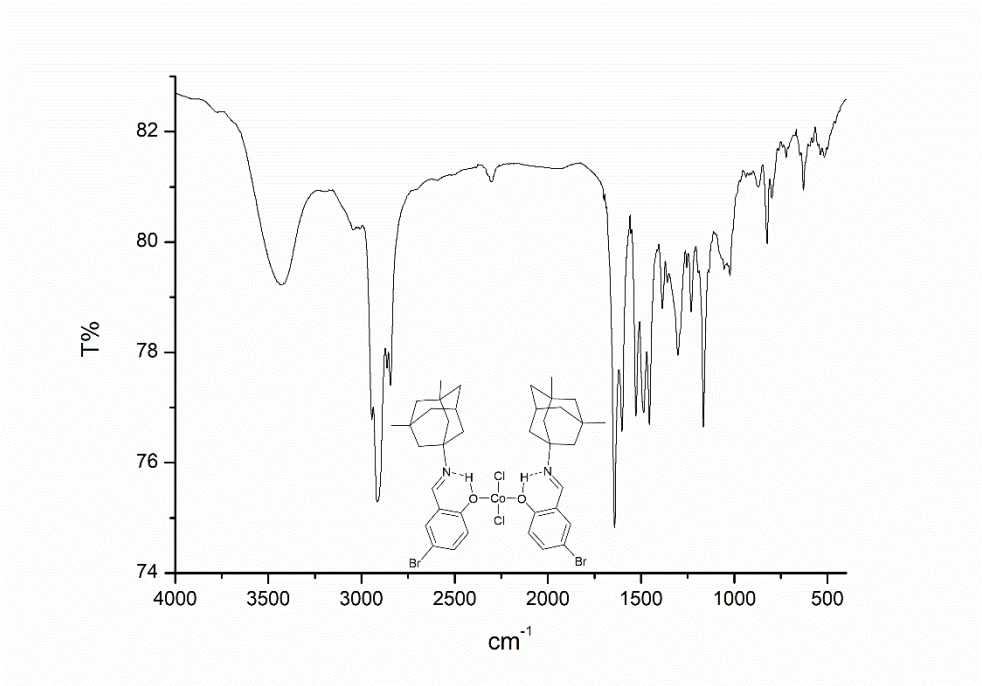

Figure S28. IR of $CoCl_2(HL4)_2$.

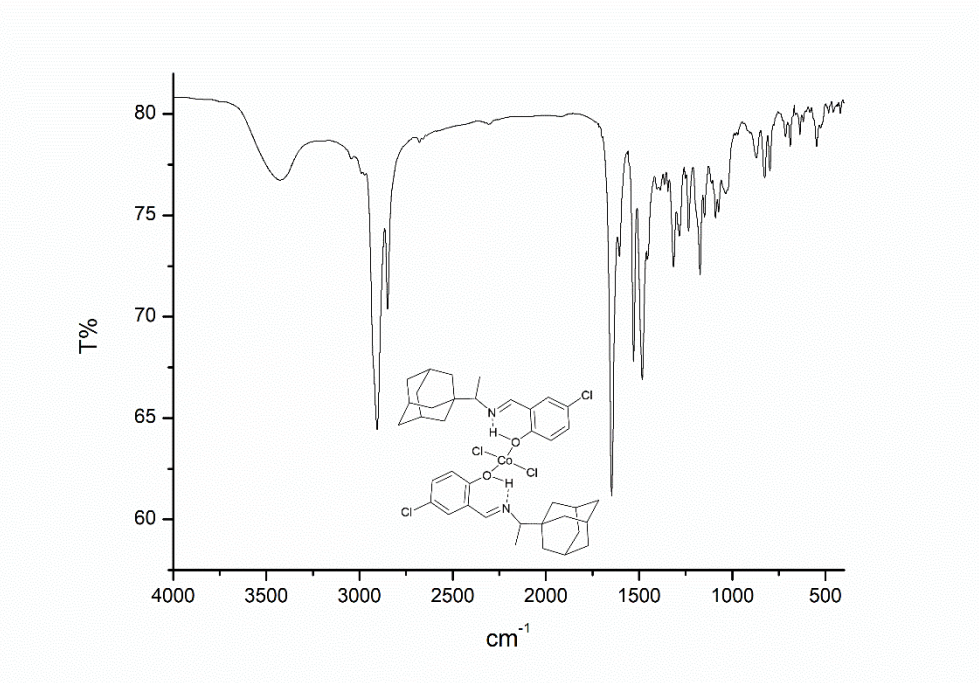

Figure S29. IR of $CoCl_2(HL5)_2$.

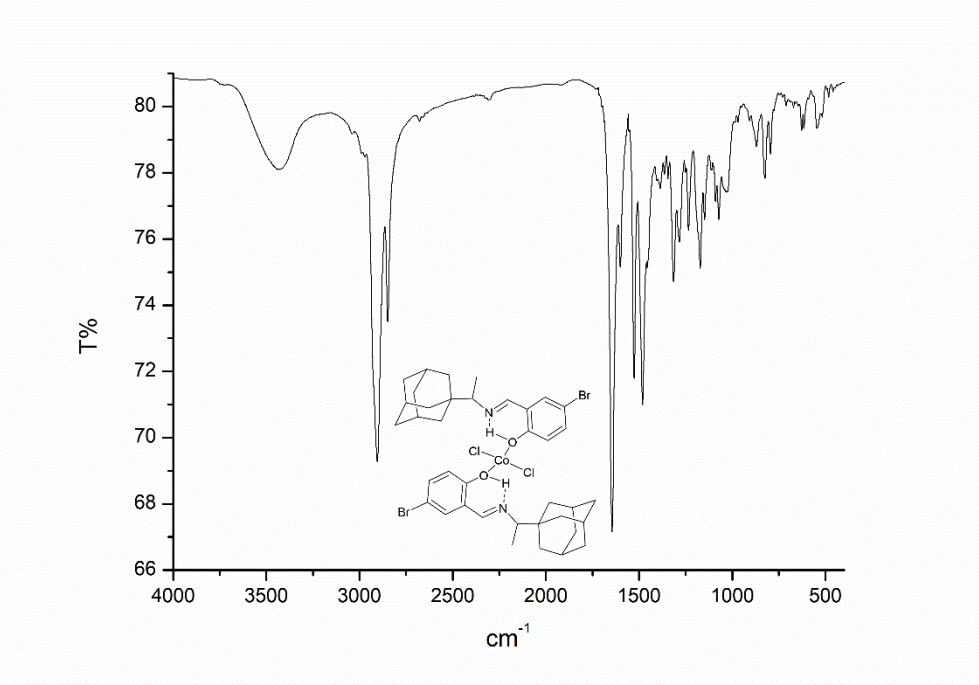

Figure S30. IR of $CoCl_2(HL6)_2$.

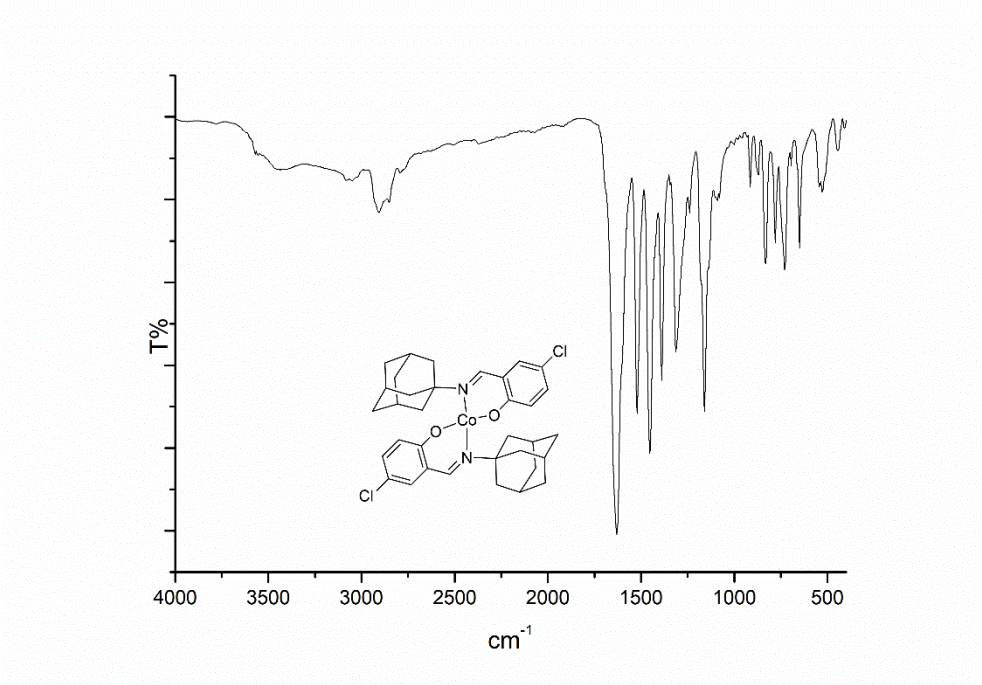

Figure S31. IR of $\mathbf{CoL1_2}$.

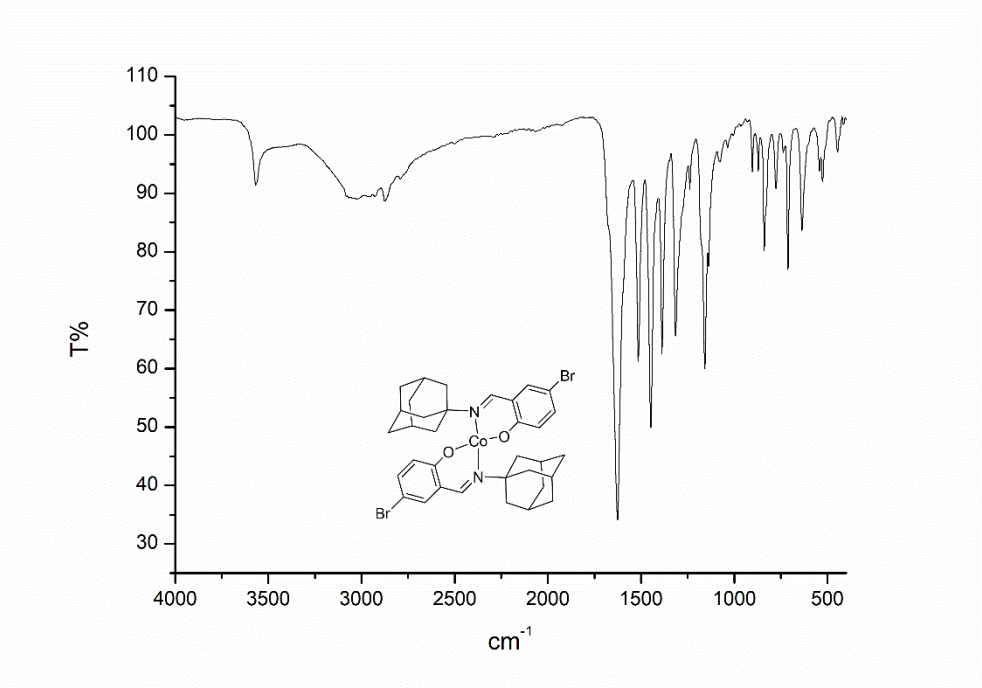

Figure S32. IR of $\mathbf{CoL2_2}$.

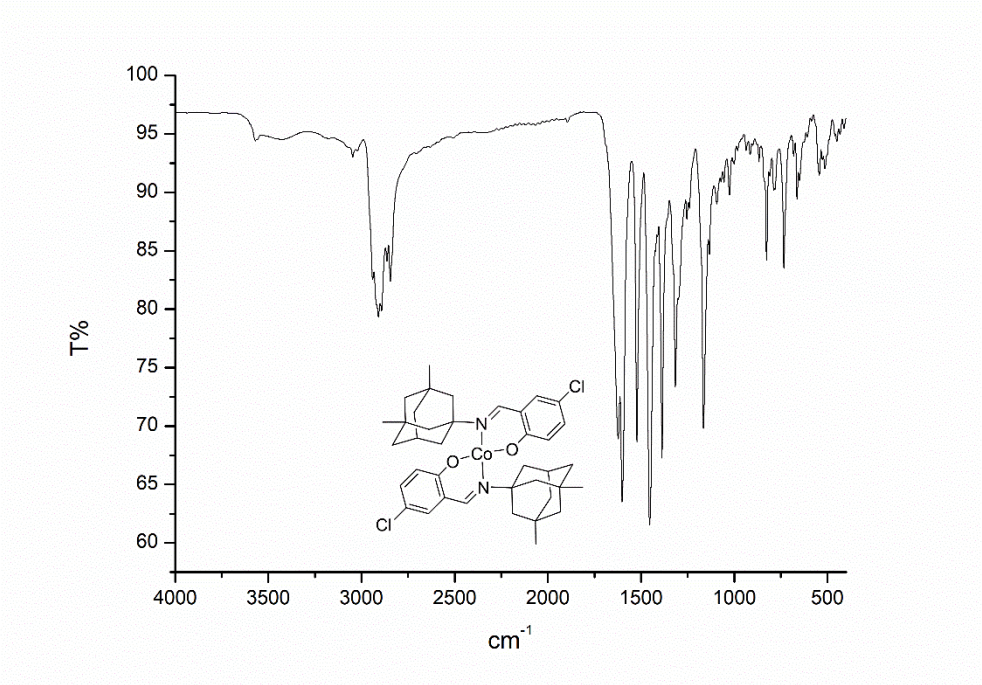

Figure S33. IR of **$CoL3_2$**.

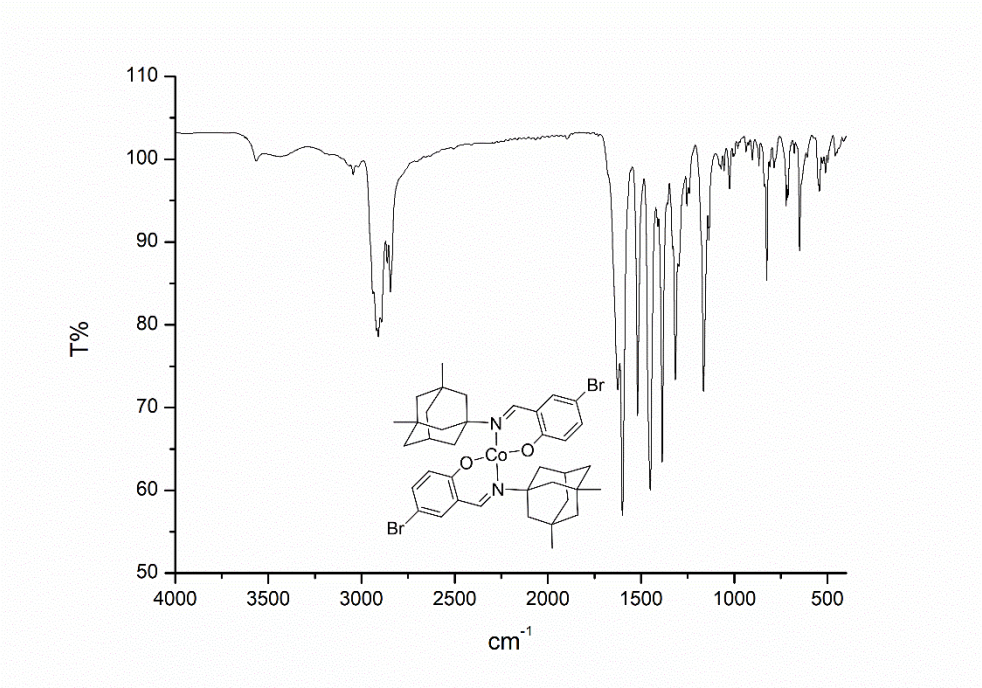

Figure S34. IR of **$CoL4_2$**.

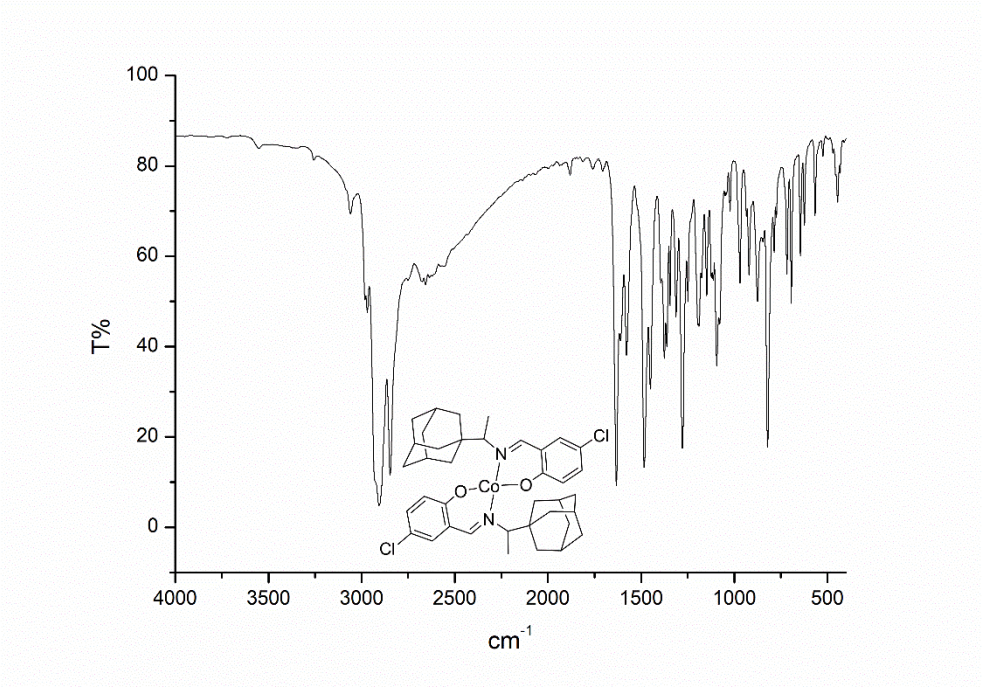

Figure S35. IR of **$CoL5_2$**.

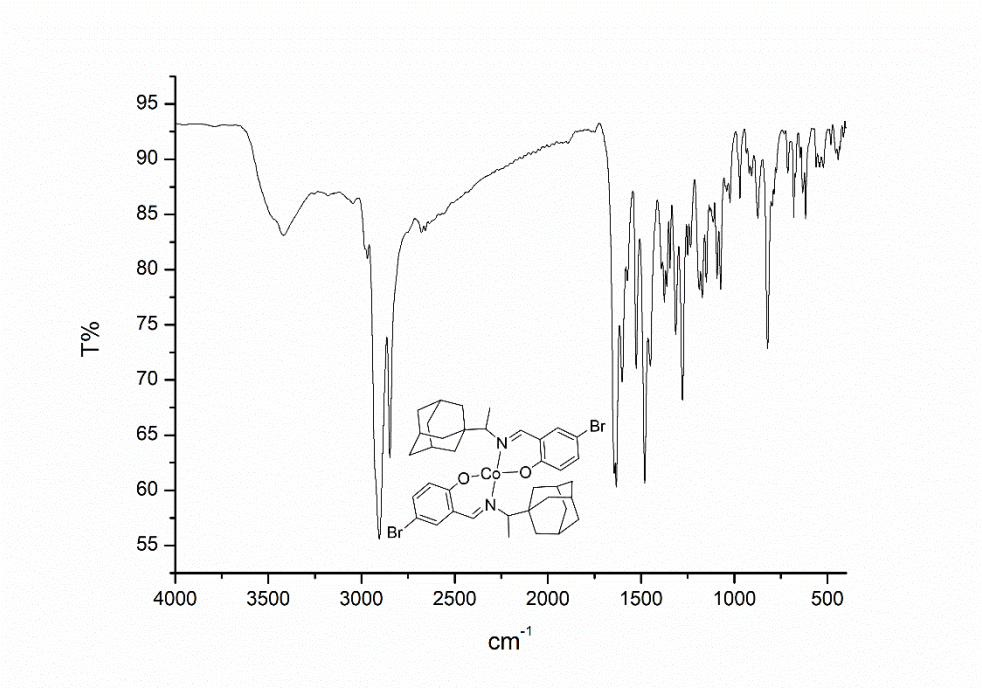

Figure S36. IR of **$CoL6_2$**.

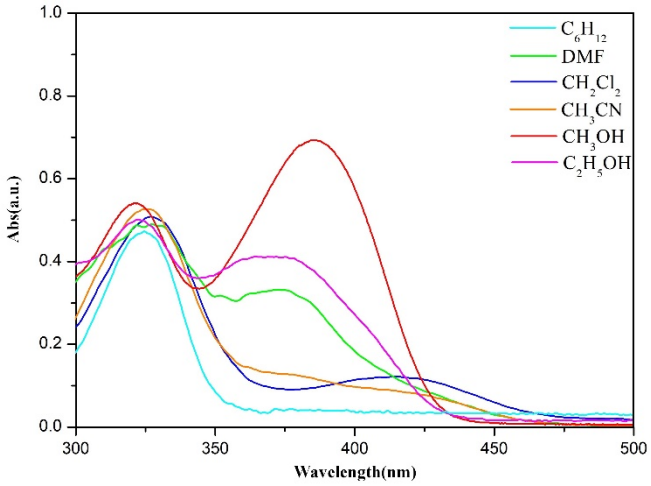

Figure S37. UV absorption spectra of $CoCl_2(HL1)_2$ in six solvents.

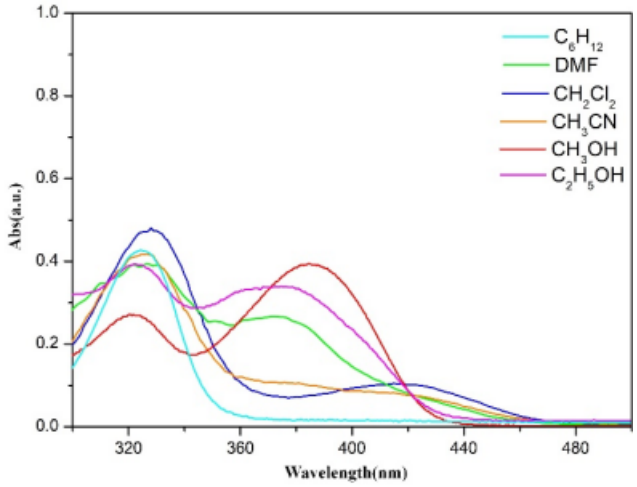

Figure S38. UV absorption spectra of $CoCl_2(HL2)_2$ in six solvents.

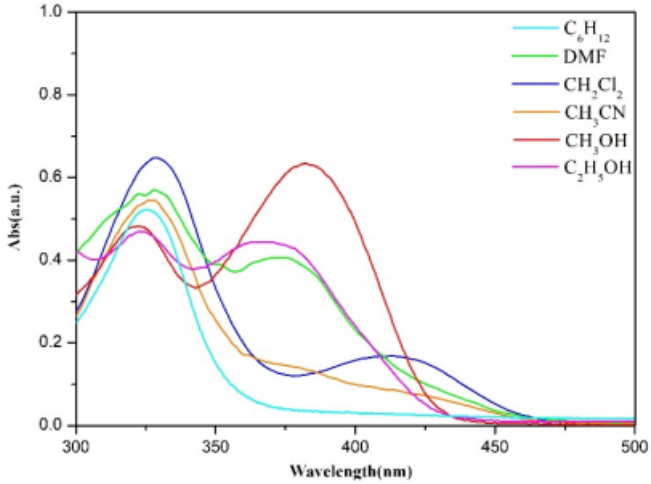

Figure S39. UV absorption spectra of $CoCl_2(HL3)_2$ in six solvents.

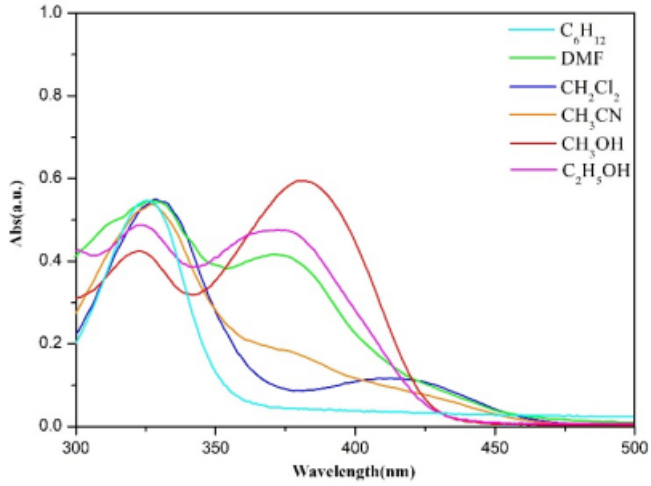

Figure S40. UV absorption spectra of $CoCl_2(HL4)_2$ in six solvents.

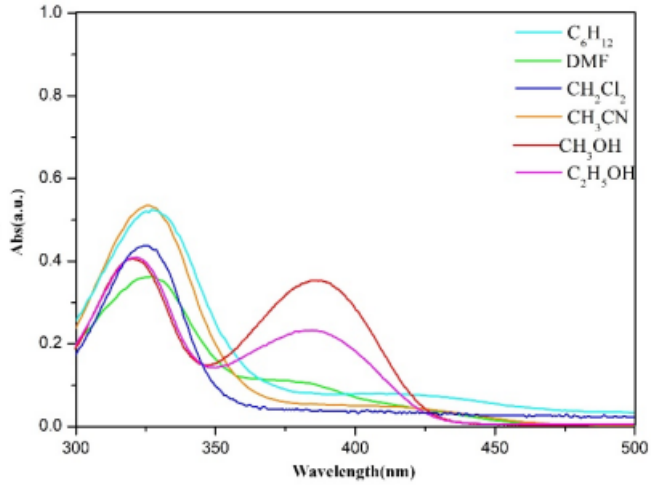

Figure S41. UV absorption spectra of $CoCl_2(HL5)_2$ in six solvents.

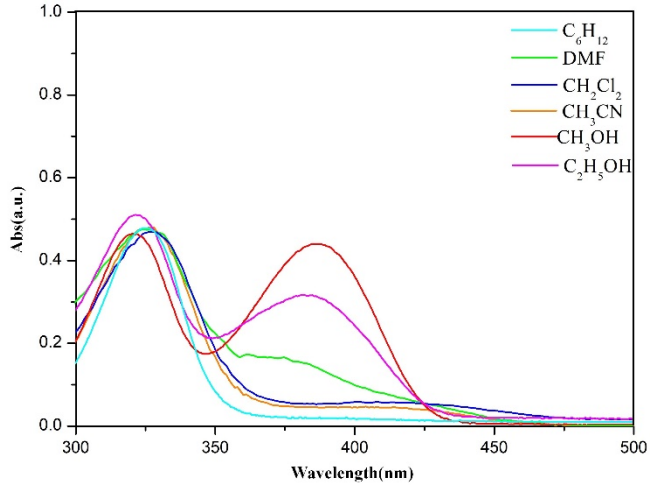

Figure S42. UV absorption spectra of $CoCl_2(HL6)_2$ in six solvents.

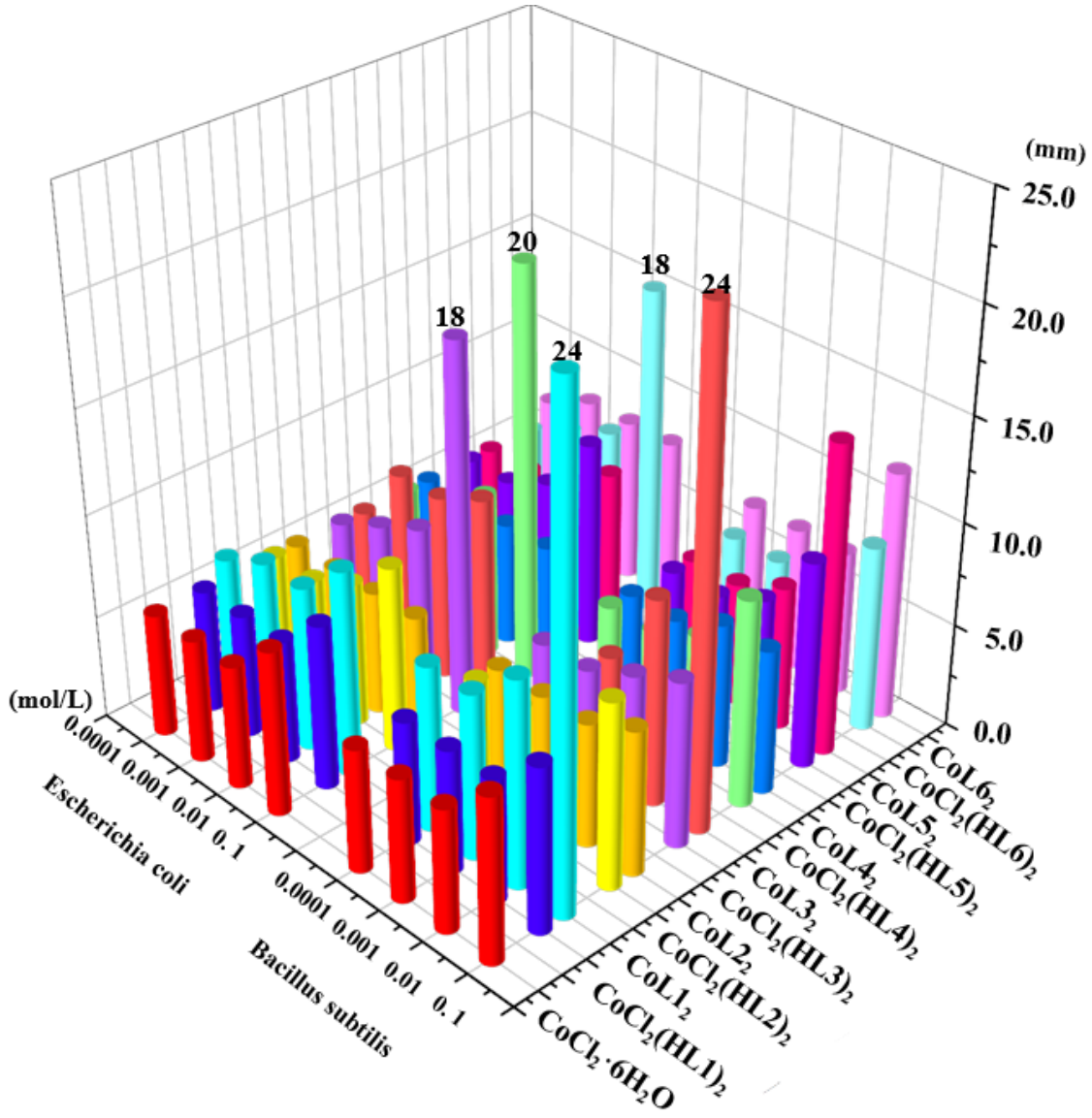

Figure S43. Antimicrobial activity of $CoCl_2(HL)_2$ and CoL_2 (**L=L1-L6**) samples against *Escherichia coli* and *Bacillus subtilis*.

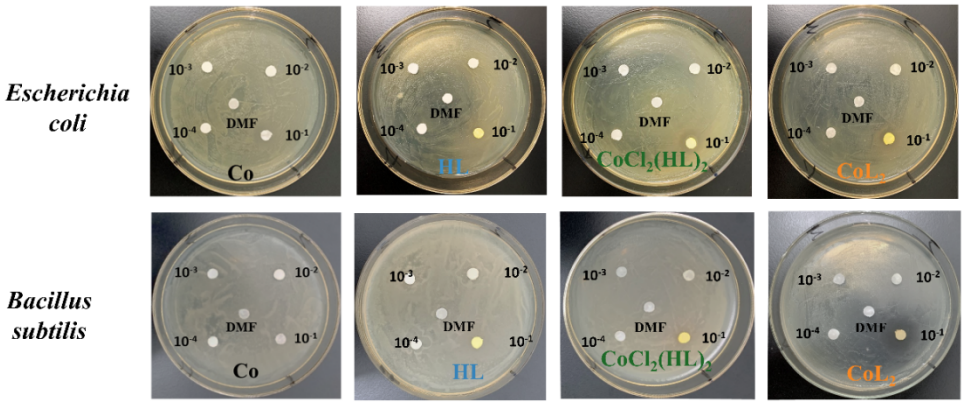

Figure S44. Circle of inhibition images illustrating the superior antimicrobial activity of $CoCl_2(HL)_2$ and CoL_2 (where L = **L1-L6**) samples against *Escherichia coli* and *Bacillus subtilis*.

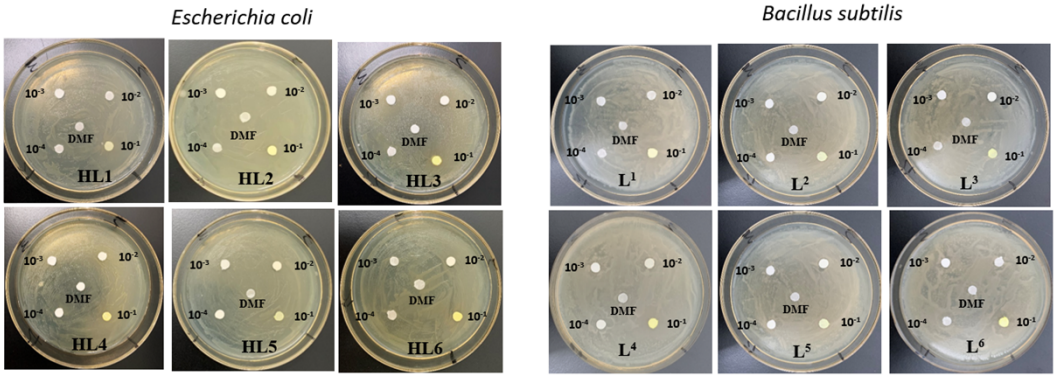

Figure S45. Circle of inhibition images illustrating the superior antimicrobial activity of **HL1-HL6** samples against *Escherichia coli* and *Bacillus subtilis*.

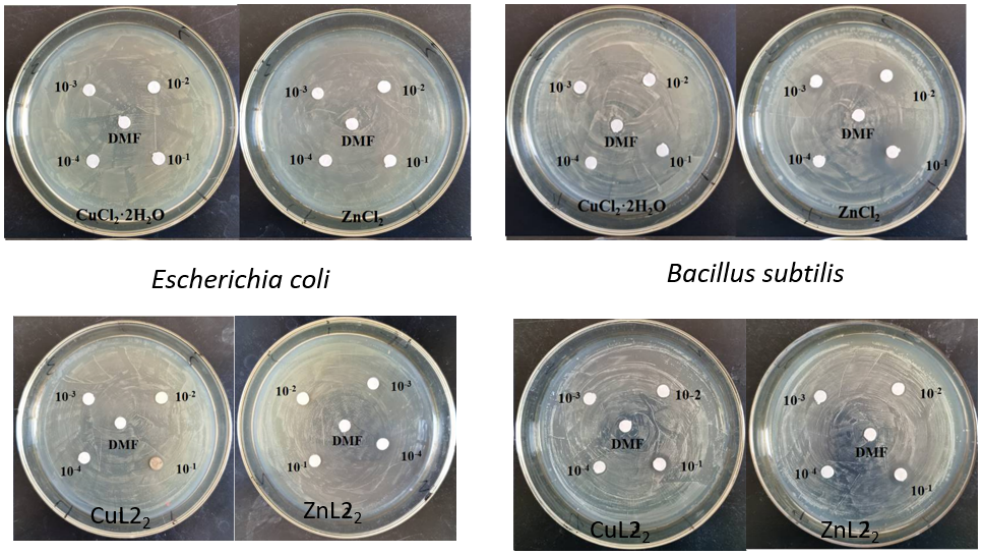

Figure S46. The inhibition image circles illustrate the superior antimicrobial activity of CuL_2 and ZnL_2 samples against *Escherichia coli* and *Bacillus subtilis*.

Table S1. Crystal data and structural refinement parameters for **$CoCl_2(HL)_2$ (L=L1-L4)**.

	$CoCl_2(HL1)_2$•CH_3CN	**$CoCl_2(HL2)_2$•CH_3CN**	**$CoCl_2(HL3)_2$**	**$CoCl_2(HL4)_2$**
Empirical formula	$C_{34}H_{40}Cl_4CoN_2O_2$ •CH_3CN	$C_{34}H_{40}Br_2Cl_2CoN_2O_2$ •CH_3CN	$C_{38}H_{48}Cl_4CoN_2O_2$	$C_{38}H_{48}Br_2Cl_2CoN_2O_2$
Formula weight ($g \cdot mol^{-1}$)	750.46	839.38	765.56	854.46
T/K	298.15	298.15	298.15	298.15
Crystal system	Monoclinic	Monoclinic	Monoclinic	Monoclinic
Space group	$P2_1/c$	$P2_1/c$	$P2_1/c$	$P2_1/c$
a (*Å*)	11.0447 (7)	11.0506 (10)	10.5886 (8)	10.6891 (5)
b (*Å*)	19.8359 (12)	19.9712 (16)	20.5254 (14)	20.7994 (11)
c (*Å*)	17.1800 (10)	17.2804 (14)	17.5615 (12)	17.7270 (9)
α (°)	90.00	90.00	90.00	90.00
β (°)	105.830 (2)	105.567 (4)	99.442 (3)	99.970 (2)
γ (°)	90.00	90.00	90.00	90.00
V ($Å^3$)	3621.1 (4)	3673.8 (5)	3765.0 (5)	3881.7 (3)
Z	4	4	4	4
θ range (°)	3.209 – 28.332	2.860–28.230	2.893 – 28.410	2.930–28.224
ρ ($g\ cm^{-3}$)	1.377	1.518	1.3505	1.4620
μ (mm^{-1})	0.805	2.823	0.775	2.673
Reflections collected/Unique	60851/8939 [R (int) = 0.0386]	38890/6420 [R (int) = 0.0644]	52969/6523 [R (int) = 0.1056]	71480/9653 [R (int) = 0.0581]
Data/restraints/parameters	8939/0/416	6420/0/416	6523/0/428	9653/2/428
Goodness-of-fit (GoF)	1.092	1.162	1.105	1.030
F (000)	1564.0	1708	1608.2775	1748.9386
R_1[a]/wR_2[b] ($I > 2\sigma(I)$)	0.0584/0.1228	0.0717/0.1117	0.1076/0.2130	0.0506/0.1161
R_1/wR_2 (all data)	0.0728/0.1294	0.1055/0.1266	0.1435/0.2277	0.0825/0.1298

[a] $R_1 = \Sigma||F_o|-|F_c||/|F_o|$, [b] $wR_2 = [\Sigma w(F_o^2-F_c^2)^2/\Sigma w(F_o^2)^2]^{1/2}$

Table S2. Crystal data and structural refinement parameters for **$CoCl_2(HL5)_2$** and **$CoCl_2(HL6)_2$**.

	$CoCl_2(HL5)_2$	**$CoCl_2(HL6)_2$**
Empirical formula	$C_{38}H_{48}Cl_4CoN_2O_2$	$C_{38}H_{48}Br_2Cl_2CoN_2O_2$
Formula weight ($g \cdot mol^{-1}$)	765.56	854.46
T/K	298.15	298.15
Crystal system	Monoclinic	Monoclinic
Space group	*C*2/*c*	*C*2/*c*
a (Å)	14.8873 (9)	14.9582 (7)
b (Å)	11.7206 (8)	11.8685 (6)
c (Å)	21.8361 (18)	21.8710 (10)
α (°)	90.00	90.00
β (°)	97.039 (3)	96.712 (2)
γ (°)	90.00	90.00
V ($Å^3$)	3781.4 (5)	3856.2 (3)
Z	4	4
θ range (°)	2.796 – 28.358	2.991–28.268
ρ ($g\ cm^{-3}$)	1.3446	1.4717
μ (mm^{-1})	0.772	2.690
Reflectionscollected/Unique	28781/3310 [R (int) = 0.0401]	33669/4785 [R (int) = 0.0355]
Data/restraints/parameters	3310/0/214	4383/0/206
Goodness-of-fit (GoF)	1.049	1.057
F (000)	1608.2775	1748.9386
R_1 [a]/wR_2 [b] ($I > 2\sigma(I)$)	0.0446/0.1077	0.0432/0.1039
R_1/wR_2 (all data)	0.0522/0.1120	0.0531/0.1089

[a] $R_1 = \Sigma||F_o|-|F_c||/|F_o|$, [b] $wR_2 = [\Sigma w(F_o^2-F_c^2)^2/\Sigma w(F_o^2)^2]^{1/2}$

Table S3. Crystal data and structural refinement parameters for **$CoL2_2$**, **$CoL3_2$**, **$CoL5_2$** and **$CoL6_2$**.

	$Co(L2)_2$·DMSO	**$Co(L3)_2$**	**$Co(L5)_2$**	**$Co(L6)_2$**
Empirical formula	$C_{34}H_{38}Br_2CoN_2O_2$ ·DMSO	$C_{38}H_{46}Cl_2CoN_2O_2$	$C_{38}H_{46}Cl_2CoN_2O_2$	$C_{38}H_{46}Br_2CoN_2O_2$
Formula weight ($g \cdot mol^{-1}$)	803.54	692.60	756.62	845.53
T/K	298	298.15	293.15	293.15
Crystal system	Triclinic	Orthorhombic	Monoclinic	Monoclinic
Space group	$P\bar{1}$	*P b c a*	$P2_1/c$	$P2_1/c$
a (Å)	9.2599 (18)	11.9064 (11)	9.2609 (3)	9.3452 (6)
b (Å)	11.641 (2)	21.691 (2)	19.2802 (5)	19.3896 (2)
c (Å)	17.466 (4)	27.191 (3)	21.3356 (6)	21.2518 (17)
α (°)	86.435 (10)	90.00	90.00	90.00
β (°)	87.209 (10)	90.00	98.987 (3)	99.125 (6)
γ (°)	70.237 (9)	90.00	90.00	90.00
V ($Å^3$)	1767.6 (6)	7022.3(11)	3762.75(19)	3802.1 (5)
Z	2	8	4	4
θ range (°)	5.834–56.72	2.929 – 29.179	2.32 – 25.00	2.44–25.00
ρ ($g\ cm^{-3}$)	1.510	1.310	2.122	3.813
μ (mm^{-1})	2.842	0.676	4.420	17.768
Reflections collected/Unique	2842 / 8787 [R (int) = 0.0412]	13086 / 9457 [R(int) = 0.0373]	14275 / 6600 [R(int) = 0.0247]	14955 / 6686 [R (int) = 0.0554]
Data/restraints/parameters	8787/0/408	9457/0/410	6686/1/433	6686/1/433
Goodness-of-fit (GoF)	1.028	1.115	1.056	1.056
F (000)	822.0	2920.0	2310.0	4032.0
R_1[a]/wR_2[b] ($I > 2\sigma(I)$)	0.0603/0.1508	0.0459/ 0.1088	0.0562/ 0.1694	0.0713/0.1785
R_1/wR_2 (all data)	0.0909/0.1654	0.0611/ 0.1217	0.0754/ 0.1898	0.1420/0.2183

[a] $R_1 = \Sigma||F_o|-|F_c||/|F_o|$, [b] $wR_2 = [\Sigma w(F_o^2-F_c^2)^2/\Sigma w(F_o^2)^2]^{1/}$

Table S4. Inhibitory of compounds against bacteria growth (mm).

Complexes and Bacteria name		Diameter of bacterial inhibition circles (mm)			
		1.0×10^{-1}	1.0×10^{-2}	1.0×10^{-3}	1.0×10^{-4}
Bacillus subtilis	$CoCl_2(HL1)_2$	8.0	6.0	6.0	6.0
	$CoCl_2(HL2)_2$	9.0	7.0	6.0	6.0
	$CoCl_2(HL3)_2$	8.0	7.0	6.0	6.0
	$CoCl_2(HL4)_2$	10.0	7.0	6.0	6.0
	$CoCl_2(HL5)_2$	10.0	7.0	6.0	6.0
	$CoCl_2(HL6)_2$	9.0	6.0	6.0	6.0
	$CoCl_2 \cdot 6H_2O$	8.0	6.0	6.0	6.0
	$CoL1_2$	24.0	10.0	8.0	8.0
	$CoL2_2$	7.0	6.0	6.0	6.0
	$CoL3_2$	24.0	10.0	6.0	6.0
	$CoL4_2$	7.0	7.0	6.0	6.0
	$CoL5_2$	15.0	7.0	6.0	6.0
	$CoL6_2$	12.0	7.0	7.0	7.0
Escherichia coli	$CoCl_2(HL1)_2$	8.0	6.0	6.0	6.0
	$CoCl_2(HL2)_2$	9.0	7.0	6.0	6.0
	$CoCl_2(HL3)_2$	18.0	8.0	7.0	6.0
	$CoCl_2(HL4)_2$	20.0	8.0	6.0	6.0
	$CoCl_2(HL5)_2$	10.0	7.0	6.0	6.0
	$CoCl_2(HL6)_2$	16.0	8.0	7.0	6.0
	$CoCl_2 \cdot 6H_2O$	8.0	6.0	6.0	6.0
	$CoL1_2$	10.0	8.0	8.0	7.0
	$CoL2_2$	6.0	6.0	6.0	6.0
	$CoL3_2$	10.0	9.0	9.0	6.0
	$CoL4_2$	6.0	6.0	6.0	6.0
	$CoL5_2$	8.0	7.0	6.0	6.0
	$CoL6_2$	8.0	8.0	8.0	7.0

Table S5. Comparison of yield, time, and solvent amount for mechanochemical synthesis of complexes with those reported in the literature for solvothermal methods.

	Synthesis method	Reaction time (min)	Temperature (°C)	Solvent (μL)	Yeild (%)
$CoCl_2(HL)_2$	Mechanochemical One-Pot Synthesis	10	25	Solvent-free	88 ± 2
	Solution-based syntheses	120	60	Methanol (120000)	0
CoL_2	Mechanochemical One-Pot Synthesis	10	25	Methanol (60)	87 ± 2
	Solution-based syntheses	120	60	Methanol (120000)	78 ± 2